Received: 10 September 2022 | Revised: 31 January 2023 | Accepted: 15 March 2023

DOI: 10.1111/bph.16077

RESEARCH ARTICLE

# Targeting mitochondrial stress with Szeto-Schiller 31 prevents experimental abdominal aortic aneurysm: Crosstalk with endoplasmic reticulum stress

Miquel Navas-Madroñal[1] | Rafael Almendra-Pegueros[1] | Lidia Puertas-Umbert[1] | Francesc Jiménez-Altayó[2] | Josep Julve[1,3] | Belén Pérez[2] | Marta Consegal-Pérez[1] | Modar Kassan[4] | José Martínez-González[5,6] | Cristina Rodriguez[1,6] | María Galán[1,6,7]

[1]Institut d'Investigació Biomèdica Sant Pau (IIB Sant Pau), Barcelona, Spain

[2]Department of Pharmacology, Toxicology and Therapeutics, Neuroscience Institute, Faculty of Medicine, Universidad Autónoma de Barcelona, Bellaterra, Barcelona, Spain

[3]CIBER de Diabetes y Enfermedades Metabólicas Asociadas (CIBERDEM), Instituto de Salud Carlos III, Madrid, Spain

[4]College of Dental Medicine, Lincoln Memorial University, Knoxville, Tennessee 37917, USA

[5]Instituto de Investigaciones Biomédicas de Barcelona-Consejo Superior de Investigaciones Científicas (IIBB-CSIC), IIB Sant Pau, Barcelona, Spain

[6]Centro de Investigación Biomédica en Red de Enfermedades Cardiovasculares (CIBERCV), Instituto de Salud Carlos III, Madrid, Spain

[7]Department of Basic Sciences of Health, Area of Biochemistry and Molecular Biology, University Rey Juan Carlos, 28922 Alcorcón, Spain

**Correspondence**
María Galán and Cristina Rodriguez, Institut d'Investigació Biomèdica Sant Pau (IIB Sant Pau), C/Sant Quintí, 77–79, 08041 Barcelona, Spain.
Email: maria.galana@urjc.es, mgalana@santpau.cat and crodriguezs@santpau.cat

## Abstract

**Background and Purpose:** Mitochondrial dysfunction and inflammation contribute to a myriad of cardiovascular diseases. Deleterious crosstalk of mitochondria and persistent endoplasmic reticulum (ER) stress triggers oxidative stress, which is involved in the development of vascular diseases. This study determined if inhibition of mitochondrial stress reduces aneurysm development in angiotensin II (Ang II)-infused apolipoprotein-E-deficient ($ApoE^{-/-}$) mice and its effect on ER stress.

**Experimental Approach:** The mitochondria-targeted tetrapeptide, Szeto-Schiller 31 (SS31), ameliorated mitochondrial dysfunction and the enhanced expression of ER stress markers triggered by Ang II in $ApoE^{-/-}$ mice, and limited plasmatic and vascular reactive oxygen species (ROS) levels. Interestingly, SS31 improved survival, reduced the incidence and severity of abdominal aortic aneurysm (AAA), and the Ang II-induced increase in aortic diameter as evaluated by ultrasonography, resembling the response triggered by the classic ER stress inhibitors tauroursodeoxycholic acid (TUDCA) and 4-phenylbutyrate (PBA).

**Key Results:** Disorganization of the extracellular matrix, increased expression of metalloproteinases and pro-inflammatory markers and infiltration of immune cells induced by Ang II in the abdominal aorta were effectively reduced by SS31 and ER inhibitors. Further, C/EBP homologous protein (CHOP) deficiency in $ApoE^{-/-}$ mice attenuated Ang II-mediated increase in vascular diameter and incidence of AAA, suggesting its contribution to the favourable response induced by ER stress inhibition.

**Abbreviations:** AAA, abdominal aortic aneurysm; Ang II, angiotensin II; ATF6, activating transcription factor 6; CHOP, C/EBP homologous protein; IRE1, inositol-requiring enzyme 1; LAMP-2, lysosome-associated membrane protein 2; MMP, metalloproteinase; PERK, protein kinase R (PKR)-like endoplasmic reticulum kinase; SS31, Szeto-Schiller 31; UPR, unfolding protein response.

Cristina Rodriguez and María Galán contributed equally.

**Funding information**
Instituto de Salud Carlos III (ISCIII), Grant/Award Numbers: PI17/01837, PI20/01004, PI21/01048, CP15/00126, FI21/00125, FI19/00331, CP20/01004

**Conclusions and Implications:** Our data demonstrate that inhibition of mitochondrial stress by SS31 limits AAA formation and increases survival through a reduction of vascular remodelling, inflammation and ROS, and support that attenuation of ER stress contributes to the favourable response elicited by SS31.

**KEYWORDS**
ageing, antioxidants, hypertension, in vivo, inflammation, small molecules, translational pharmacology, vascular pharmacology

## 1 | INTRODUCTION

Abdominal aortic aneurysm (AAA) is an age-related and commonly asymptomatic degenerative disorder, with high morbidity and mortality (Nordon et al., 2011; Weintraub, 2009). The prevalence of AAA is 4%–8% in the male population aged over 65 years, whereas the prevalence is three to five times lower in women. Aneurysm rupture is the most severe consequence of this disease, being a worldwide leading cause of death (GBD, 2015; Kuivaniemi et al., 2015). Unfortunately, there are no pharmacological tools able to halt the expansion of AAA. In fact, currently, the management of AAA relies exclusively on surgical repair by open surgery, or endovascular repair of those aneurysms with elevated risk of rupture, where aneurysm diameter is the principal surrogate marker for disease progression (Klink et al., 2011; Ulug et al., 2020).

The implementation of ultrasound screening programmes has allowed an early diagnosis of this disease (Golledge, 2019; Kuivaniemi et al., 2015), supporting the need for pharmacological interventions to slow AAA expansion and/or reduce aneurysm rupture. However, none of the pharmacological strategies evaluated to date have conclusively demonstrated any clinical benefit (Baxter et al., 2020; Emeto et al., 2014; Samson, 2012). Therefore, major clinical challenges include the development of rational pharmacological therapeutic approaches to effectively limit AAA progression and rupture. To achieve these objectives, it is essential to delve into the pathogenesis of AAA, which is characterized by degradation of the extracellular matrix (ECM), chronic inflammation, oxidative stress, and vascular smooth muscle cell (VSMC) apoptosis (Potteaux & Tedgui, 2015; Shimizu et al., 2006). Besides the main risk factors (such as ageing, male sex and smoking history), hypertension also is a major public health problem associated with the presence of AAA (Torres-Fonseca et al., 2019). Patients with AAA show an enhanced risk of cardiovascular mortality, including that triggered by cardiac disorders closely linked with hypertension (Bath et al., 2015; Forsdahl et al., 2010; Freiberg et al., 2008).

Processes critically involved in the pathogenesis of AAA (including inflammation, hypoxia and an exacerbated generation of reactive oxygen species (ROS)), perturb mitochondria functionality and endoplasmic reticulum (ER) homeostasis (Navas-Madroñal et al., 2019; Qin et al., 2017; Tabas & Ron, 2011; Timmins et al., 2009). Mitochondrial dysfunction and ER stress are closely related, and their deleterious crosstalk promotes mitochondrial ROS generation and apoptosis (Giorgi et al., 2009; Malhotra & Kaufman, 2007). Indeed, we have previously demonstrated that mitochondrial function is disturbed in cases of human AAA and that mitochondrial dysfunction is connected to ER stress in patients with this disease (Hetz et al., 2020). Chronic ER stress activation leads to mitochondria-dependent apoptosis through the protein kinase R (PKR)-like endoplasmic reticulum kinase (**PERK**) and activation of transcription factor 6 (ATF6) pathways of the unfolding protein response (UPR), by promoting the expression of the pro-apoptotic factor C/EBP homologous protein (CHOP; or DDIT3) and through the inositol-requiring enzyme 1 (**IRE1**)–UPR pathway (Hetz et al., 2020; Tabas & Ron, 2011; Timmins et al., 2009).

### What is already known

- Abdominal aortic aneurysm is a disease for which there is no effective pharmacological treatment.
- Mitochondrial and endoplasmic reticulum stress are induced in cardiovascular diseases like AAA and cardiac hypertrophy.

### What does this study add

- Inhibition of either mitochondrial stress or ER stress prevents AAA formation, by reducing cardiovascular remodelling.
- The mitochondria-targeted peptide, SS31, as well as CHOP deficiency reduces aortic remodelling underlying AAA formation.

### What is the clinical significance

- Targeting mitochondrial or ER stress by different approaches prevents the AAA formation and cardiovascular remodelling.
- Targeting mitochondrial and ER stress are valuable therapeutic approaches for managing aortic aneurysm.

Targeting mitochondrial dysfunction by the mitochondria-targeted tetrapeptide D-Arg-2′,6′-dimethyltyrosine-Lys-Phe-$NH_2$, also known as Szeto-Schiller 31 (SS31), has demonstrated its potential benefit in vascular disorders such as ischaemia–reperfusion injury, atherosclerosis, pulmonary arterial hypertension or sepsis-induced vascular leakage (Cai et al., 2018; Lu et al., 2016; M. Zhang et al., 2017; J. Zhang, Wang, et al., 2021). The tetrapeptide SS31 improves electron transport, reduces the production of toxic ROS, and inhibits cytochrome c release (Szeto, 2008; Zhao et al., 2004). However, whether targeting mitochondrial oxidative stress with SS31 could be a useful strategy for the treatment of AAA and if this peptide could circumvent the failure of other antioxidant approaches found in clinical trials have not been previously addressed. Here, we show that targeting mitochondrial dysfunction impacts on ER stress, thereby influencing AAA formation and hypertensive cardiac hypertrophy.

## 2 | METHODS

### 2.1 | Animal handling

Animal studies are reported in compliance with the ARRIVE guidelines (Percie du Sert et al., 2020) and with the recommendations made by the *British Journal of Pharmacology* (Lilley et al., 2020). Animals were bred in the Animal Experimentation Unit (Institut de Recerca de l'Hospital de la Santa Creu i Sant Pau, Barcelona, Spain) in a controlled, specific pathogen-free environment under standard light–dark cycle (12-h light/dark cycle) and temperature (21 ± 1°C) conditions, and were fed ad libitum with a standard commercial diet (Harlan Iberica SL, Barcelona, Spain). Animal handling and disposal were performed in accordance with the principles and guidelines established by the Spanish Policy for Animal Protection RD53/2013, which meets the European Union Directive 2010/63/UE on the protection of animals used for experimental and other scientific purposes. All procedures were reviewed and approved by the local ethical committee as stated in Law 5/1995, 21 June, passed by the Generalitat de Catalunya.

The apolipoprotein-E-deficient ($ApoE^{-/-}$) mouse infused with **angiotensin II** (Ang II) was used as a model of AAA, as previously described (Daugherty et al., 2000; Galán et al., 2016). Eleven-week-old male and female $ApoE^{-/-}$ mice ($ApoE^{-/-}$; B6.129P2-Apoetm1Unc/J) were obtained from Charles River UK Ltd (Kent, UK), bred in the Animal Experimentation Unit and housed in a controlled, specific pathogen-free environment.

The CHOP-deficient mice ($CHOP^{-/-}$) were obtained from Jackson Laboratories (B6.129S(Cg)-$Ddit3^{tm2.1Dron}$/J; USA) and were bred with C57BL/6J mice in the Animal Experimentation Unit, and housed in a controlled, specific pathogen-free environment. After nine crossbreeding generations, $CHOP^{-/-}$ mice under a C57BL/6J genetic background were bred with $ApoE^{-/-}$ mice to generate double knockout (KO) mice ($ApoE^{-/-}$/$CHOP^{-/-}$).

Ang II (1000 ng·$kg^{-1}$ body weight·$min^{-1}$; Sigma-Aldrich, St. Louis, MO, USA) was infused via osmotic minipumps (model 1004, Alzet, DURECT Corporation, CA, USA) implanted subcutaneously into the interscapular space of **isoflurane**-anaesthetized mice for 28 days. About 50% of males and females were randomly distributed into different experimental groups: untreated Ang II-infused mice (n = 27); two groups of Ang II-infused $ApoE^{-/-}$mice receiving either the tetrapeptide SS31 or its inert analogue SS20 as a control (3 mg·$kg^{-1}$ body weight, Caslo peptides, Denmark) and delivered by osmotic minipump infusion (n = 18 each group); two groups of Ang II-infused mice that received an intraperitoneal injection of the classic ER stress inhibitors, tauroursodeoxycholic acid (**TUDCA**; 150 mg·$kg^{-1}$ body weight) and sodium 4-phenylbutyrate (**4-PBA**; 1 g·$kg^{-1}$ body weight; Sigma-Aldrich) (n = 17 each group) 3 days a week; a control group, $ApoE^{-/-}$ mice infused with saline (n = 15). Doses of ER stress inhibitors and route of administration were chosen according to previous studies in vivo (Dai et al., 2011; Kassan et al., 2012; Nickel et al., 2015; Qin et al., 2017). Treatments started the first day of minipump implantation. In the case of the double KO mice, animals were randomly assigned to three groups: Ang II-infused double KO males (n = 13); Ang II-infused littermates expressing CHOP ($ApoE^{-/-}$/$CHOP^{+/+}$, n = 16); and control group, double KO males infused with saline (n = 7).

For the implantation of osmotic minipumps, mice were anaesthetized with isoflurane (2%). Anaesthetic depth was confirmed by loss of blink reflex and/or lack of response to tail pinch. The procedure took about 10 min per mouse. Recovery after surgical procedures was carried out using aseptic techniques in a dedicated approved surgical area. Antibiotics (**penicillin** 450,000 µg·$kg^{-1}$, intramuscular) and analgesics (**buprenorphine** 0.05 mg·$kg^{-1}$, subcutaneous) were given immediately after surgery to prevent infection and discomfort. The animals were kept warm in a heating pad until awake after surgery, and observed carefully by the investigators throughout the post-surgery period. At the end of the experimental procedures, mice were killed via isoflurane overdose and aortas were harvested immediately, examined for the presence of an AAA, and appropriately processed for further studies.

### 2.2 | Non-invasive measurement of systolic blood pressure

Systolic blood pressure (SBP), diastolic blood pressure (DBP) and mean arterial pressure (MAP) were non-invasively measured in conscious mice prior to and following treatment, using the tail-cuff plethysmography method (CODA tail-cuff system, Kent Scientific, USA), and the acquired data were analysed with the software Coda 4. Mice were trained for tail-cuff measurements over a period of 1 week before starting with either Ang II or saline infusion. Blood pressure measurements were performed at the same time (between 9 AM and 11 AM) to avoid the influence of the circadian cycle. Mean blood pressure values were taken from 10 consecutive measurements.

## 2.3 | Basic measurements of ultrasound recording for abdominal aortas

Mice were anaesthetized with 1.5% isoflurane inhalation and were lightly secured in the supine position on a warming platform. After shaving the praecordium, an abdominal echography was performed using a Vevo 2100 ultrasound with a 30-MHz transducer applied to the abdominal wall to record abdominal aorta (VisualSonics, Toronto, ON, Canada). The maximum aortic diameter was assessed in diastole in an abdominal segment located just before the bifurcation of the left renal artery and by the same observer during the whole study period. Abdominal aortas with external diameters ≥ 1.5 mm were considered as an aneurysm. All primary measurements were made from images captured on cine loops of 100 frames at the time of the study, using the software provided by the echography machine.

The severity of the aneurysm was based on a 4-point grading scale, previously described in detail (Manning et al., 2002): type 0, no aneurysm; type I, dilated lumen in the suprarenal region of the aorta with no thrombus (blood clot); type II, remodelled tissue in the suprarenal region that frequently contained a thrombus; type III, a pronounced bulbous form of type II that contained a thrombus; type IV, a form in which there are multiple AAAs containing a thrombus.

## 2.4 | Basic measurements of cardiac function by echocardiography (M-mode and Doppler)

Anaesthetized mice (2% isoflurane) were subjected to transthoracic echocardiography, using a Vevo 2100 ultrasound unit with a 30-MHz transducer (VisualSonics), as described previously (Galán et al., 2017).

Two-dimensional and M-mode images were obtained in parasternal long-axis and short-axis views, respectively. Measurements of the interventricular septal thickness (IVS), LV internal dimension (LVID), and thickness of the LV posterior wall (LVPW) and LV anterior wall (LVAW) at diastole and systole (LVIVSd, LVIDd, LVPWd and LVAWd; and IVSs, LVIDs, LVPWs and LVAWs, respectively) were obtained. Ejection fraction (EF) and fractional shortening (FS) also were determined. To achieve diastolic function determinations, pulsed Doppler imaging was obtained from the B mode of the four-chamber view. The early filling peak velocity I, atrial peak velocity (A), E/A ratio, mitral valve ejection time (MVET) or the interval between the beginning of the E wave to the 0 baseline, aortic ejection time or LV ejection time, and isovolumetric relaxation time (IVRT) were determined.

## 2.5 | Total mRNA and protein isolation from tissues

After removal of adventitial fat from mouse aortas, the segment of the abdominal aorta, including the aneurysmal region and the rest of the abdominal aorta up to the iliac bifurcation was separated, snap-frozen in liquid nitrogen, and stored at −80°C. Total RNA and protein isolation from mouse abdominal aortas was performed using the TriPure reagent (Roche Diagnostics, Indianapolis, IN, USA) following the manufacturer's instructions. RNA integrity was determined by electrophoresis in agarose gels and was quantified by a NanoDrop 1000 Spectrophotometer (Thermo Scientific).

## 2.6 | Real-time PCR

DNase-I-treated total RNA (1 μg) was reverse transcribed into cDNA using the High Capacity cDNA Archive Kit (Applied Biosystems, Foster City, CA, USA) with random hexamers. Quantification of mRNA levels in mouse tissues was performed by real-time PCR using an ABI PRISM 7900HT sequence detection system (Applied Biosystems) and TaqMan fluorescent real-time PCR primers, and the probes provided by Applied Biosystems or Integrated DNA technologies as follows: *Atf6* (Mm01295319_m1); *Atf4* (Mm005105325_g1); Chop (*Ddit3*; Mm01135937_g1); heat shock protein 5 (***Hspa5***; Mm00517691_m1); inositol-requiring enzyme 1 (*Ern1*; Mm00470233_m1); X-binding protein 1 (*Xbp1*; Mm00457357_m1); spliced X-binding protein 1 (*sXbp1*; Mm03464496_m1); Gadd34 (*Gadd34*; Mm00435119_m1); monocyte chemotactic protein-1 (***Ccl2***; Mm00441242_m1); cytochrome c oxidase subunit III (*Cox3*; Mm04225261_g1); dynamin-related protein 1 (*Dnm1l*; Mm01342903_m1); BCL2/adenovirus E1B 19-kDa protein-interacting protein 3 (*Bnip3*; Mm01275600_g1); interleukin 6 (***Il6***; Mm00446191_m1); interleukin-1β (***Il1β***;Mm00434228_m1); metalloproteinase 9 (**Mmp9**; MmPT.58.10100097); metalloproteinase 9 (**Mmp2**); MmPT.58.9606100); EGF-like module-containing mucin-like hormone receptor-like 1 or **F4/80** (ADGRE1) (*Emr1*; MmPT.56a.11087779); myosin heavy chain b (*Myh7*; MmPT.58.17465550.g); and atrial natriuretic peptide (**Anp**; MmPT.58.12973594.g). As endogenous controls, glyceraldehyde 3-phosphate dehydrogenase (*Gapdh*; Mm99999915_g1) and *β-actin* (Mm02619580_g1) were used and similar results were obtained by normalizing to both housekeeping genes. Quantitative RT-PCR was carried out in an ABI PRISM 7900HT Sequence Detection System (Applied Biosystems) using the following conditions: 2 min at 50°C, 10 min at 95°C followed by 40 cycles of 15 s at 95°C and 1 min at 60°C. Relative mRNA levels were determined using the $2^{-\Delta\Delta Ct}$ method.

## 2.7 | Immunohistochemistry, immunofluorescence and histology

The immuno-related procedures used comply with the recommendations made by the *British Journal of Pharmacology* (Alexander et al., 2018). Abdominal aorta segments were fixed in 4% paraformaldehyde/0.1 M of phosphate-buffered saline (PBS; pH 7.4) for 24 h and embedded in paraffin. The site of sampling was located in the middle of the suprarenal abdominal aorta where AAA develops. Aortic sections (5 μm) were deparaffinized in xylene, rehydrated in graded ethanol and treated with 0.3% **hydrogen peroxide** for 30 min to block peroxidase activity. Then, samples were blocked with 10% of normal serum and incubated with antibodies against LAMP-2/MAC3

(1:250; Santa Cruz Biotechnology Inc., Europe, Cat# sc-19991, RRID:AB_626855) and **CD3** (1:100; Agilent Technologies Co., Hamburg, Germany, Cat# A0452, RRID:AB_2335677). After washing, samples were incubated for 1 h with a biotinylated secondary antibody (Vector Laboratories, Peterborough, UK). After rinsing three times in PBS, standard Vectastain avidin–biotin peroxidase complex (ABC; Vector Laboratories) was applied, and the slides were incubated for 30 min. Colour was developed using 3,3´-diaminobenzidine (DAB) and sections were counterstained with haematoxylin before dehydration, clearing and mounting. Negative controls, in which the primary antibody was omitted, were included to test for non-specific binding. Immunofluorescence was performed by incubating the sections with anti-DNA/RNA damage mouse monoclonal antibody (1:100; Abcam Cat# ab62623, RRID:AB_940049) to detect 8-oxo-dG (8-oxo-7,-8-dihydro-2′-deoxyguanosine) at 4°C overnight after antigen retrieval, permeabilization with PBS-0.3% Triton X-100 and blocking with PBS containing 5% albumin and 5% fetal bovine serum (FBS) for 1 h at room temperature. A secondary antibody (goat anti-mouse IgG conjugated to Alexa Fluor 488, Molecular Probes, Life Technologies) was then applied for 1 h at 20–22°C. Finally, the slides were mounted with ProLong Gold antifade reagent and 4′,6-diamidino-2-phenylindole (**DAPI**) (Molecular Probes, Life Technologies, Eugene, OR, USA). For negative controls, the primary antibody was omitted. Imaging of epifluorescent staining was performed using a Leica DM6000B microscope, and images were analysed using ImageJ (NIH). Results were quantified as positive cell numbers per area in independent sections of abdominal aortas.

The histological characterization of aortic samples was performed by Masson's trichrome and sirius red staining. Furthermore, to visualize elastic fibre integrity, arterial sections were stained with orcein using a commercial kit (Casa Álvarez, Madrid, Spain). The number of ruptures per aortic section was quantified by a blinded operator.

## 2.8 | Determination of the lipid profile in plasma

The lipid profile was determined enzymatically using commercial kits adapted to a COBAS c501 autoanalyser (Roche Diagnostics, Basel, Switzerland). The lipid profile included total cholesterol (TC) and triglycerides (TGs) (Roche Diagnostics). TG determinations were corrected for the free glycerol present in plasma (cat#F6428-40ML; Sigma-Aldrich). High-density lipoprotein cholesterol (HDL-C) was measured in apolipoprotein (Apo)B-depleted plasma, obtained after precipitation with phosphotungstic acid and magnesium ions (Roche Diagnostics). Non-HDL cholesterol was calculated as the difference between TC and HDL-C.

## 2.9 | ROS quantification in plasma

2-Hydroxyethidium (2-EOH) was determined in plasma by high-performance liquid chromatography (HPLC) with fluorescence detection, as described by Laurindo et al. (2008). Briefly, 25 µl of plasma was incubated with 0.8 µM of dihydroethidine (DHE; Sigma-Aldrich) for 1 h in PBS and centrifuged at 10,000 *g* for 5 min. The supernatant was injected into the chromatographic system (mobile phase: 65% water with 0.3% trifluoroacetic acid: 35% acetonitrile; 1 ml·min$^{-1}$ flow; column kromasil C18, 5 µm, 200 × 4.6 mm, Teknokroma Analítica; 510 nm of excitation; 595 nm of emission). **Xanthine/xanthine oxidase** (XO) was used to calibrate the signal of $O^{2-}$ and the calibration curve was constructed by comparing the production of 2-EOH and the ratio of XO activity/HE concentration (85–605 nU XO·ng HE$^{-1}$). 2-EOH present in the samples was quantified by comparing with the calibration curve based on the reaction xanthine–XO in the presence of DHE following the method previously described (Sánchez-Infantes et al., 2021).

## 2.10 | Gelatin zymography

The relative enzymatic activities of MMP9 and MMP2 in murine abdominal aorta lysates were measured by zymography. Protein lysates were prepared in radioimmunoprecipitation assay (RIPA) buffer supplemented with complete protease inhibitor cocktail (Roche). Proteins (20 µg) were resolved by 10% sodium dodecyl sulfate-polyacrylamide gel electrophoresis (SDS-PAGE) copolymerized with 1 mg·ml$^{-1}$ of porcine skin type A gelatin (Sigma-Aldrich) as a substrate for MMP enzymatic activity and run at 4°C for 4–6 h. After electrophoresis, the gels were rinsed twice for 30 min at room temperature in 2.5% Triton X-100 (Sigma-Aldrich) and then incubated in substrate buffer (50 mM of Tris–HCl, 10 mM of $CaCl_2$ [Merck], 0.02% [w/v] $N_3Na$ [Fluka], pH 8) for 18–20 h at 37°C. Gels were dyed with one tablet of PhastGel™Blue R (GE Healthcare) in 10% acetic acid. Areas of gelatinolytic activity appeared as clear bands on a blue background where the protease has digested the substrate. Gels were finally scanned with a GS-800 calibrated imaging densitometer (Bio-Rad) and quantitative densitometric analysis of digested bands was performed using Quantity-One software (Bio-Rad).

## 2.11 | Western blot (WB)

Abdominal aorta lysates obtained following TriPure reagent protocol were homogenized using a Tissue Ruptor II (Qiagen) in a RIPA buffer (150 mM of NaCl, 1% [v/v] Triton X-100, 0.5% 113 [w/v] sodium deoxycholate, 0.1% [w/v] SDS, 2 mM of ethylenediaminetetraacetic acid [EDTA], 50 mM Tris–HCl, pH 8) following a standard protocol. Total proteins were quantified using Pierce™ Bicinchoninic Acid (BCA) Protein Assay Kit (Thermo Fisher). For WB assays, the protein extracts were boiled for 5 min in Laemmli buffer 1X (125 mM of Tris–HCl, 2% SDS, 5% glycerol, 0.003% bromophenol blue and 1% β-mercaptoethanol) as a previous step to electrophoresis resolution under reducing conditions on an SDS-PAGE (gels of 10% acrylamide:bis-acrylamide 37.5:1) in parallel with a molecular weight marker and transferred to polyvinylidene fluoride (PVDF) membranes (Immobilon-P, 0.45 µM of

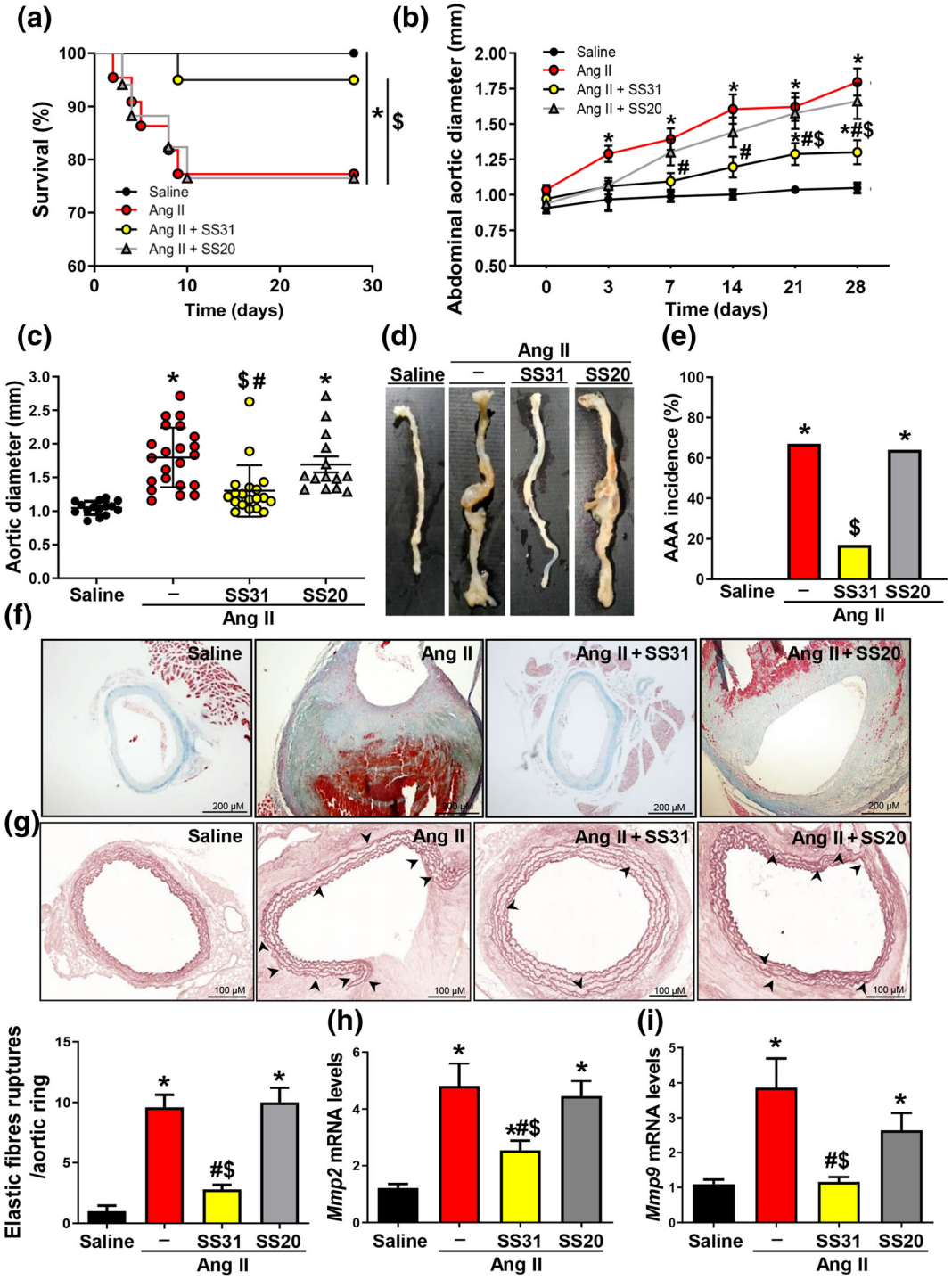


**FIGURE 1** Legend on next page.

pore; Millipore). After blocking 5% nonfat dry milk, the membrane was incubated overnight at 4°C with antibodies directed against ATF6 (NBP1-40256, RRID:AB_2058774) and XBP1 (NBP1-77681, RRID:AB_11010815) which were purchased from Novus Biologicals (Bio-Techne LD-R&D Systems Europe Ltd, Abingdon, UK), whereas the antibody against ATF4 (ab216839) was purchased from Abcam (Netherlands). The next day, the membranes were washed and were incubated (1 h at room temperature) with appropriate horseradish peroxidase-conjugated secondary antibodies (Dako Products, Agilent, Santa Clara, CA, USA). The Luminata TM Western HRP Substrate (Immobilon, Merck-Millipore) was used to detect bound antibodies. The size of detected proteins was estimated using protein molecular-mass standards. GAPDH (EMD Milipore Corp, USA, Cat# MAB374, RRID:AB_2107445) was used as a loading control.

### 2.12 | Statistical analysis

The data and statistical analysis comply with the recommendations of the *British Journal of Pharmacology* on experimental design and analysis in pharmacology (Curtis et al., 2022). GraphPad Prism 4.0 software (GraphPad, USA) was used for statistical analysis. Data were expressed as mean ± SEM and values of $P < 0.05$ were considered significant. When data fitted a normal distribution, differences among groups were assessed using one-way analysis of variance (ANOVA), with Bonferroni's test or Tukey's post hoc test for multiple comparisons. When normality failed, the Kruskal–Wallis test was applied for multiple comparisons. Differences in the trends for mortality between groups were determined using the Kaplan–Meier test, and differences in the percentage of incidence of AAA were analysed by the chi square test ($\chi^2$).

### 2.13 | Materials

Details of materials and suppliers are provided in specific subsections of Methods.

### 2.14 | Nomenclature of targets and ligands

Key protein targets and ligands in this article are hyperlinked to corresponding entries in http://www.guidetopharmacology.org and are permanently archived in the Concise Guide to PHARMACOLOGY 2021/22 (Alexander, Fabbro, et al., 2021; Alexander, Kelly, et al., 2021).

## 3 | RESULTS

### 3.1 | The mitochondria-targeted peptide SS31 reduces abdominal aorta aneurysm formation through a decrease in vascular remodelling and inflammation

We have previously demonstrated that mitochondrial dysfunction is a feature of human AAA (Navas-Madroñal et al., 2019). Because mitochondrial dysfunction and ROS generation are tightly linked with ER stress, we assessed whether SS31 influences AAA formation and if this peptide modulates ER stress in the Ang II-infused ApoE$^{-/-}$ mouse.

The percentage of Ang II-infused ApoE$^{-/-}$ mice that survived over the course of the study was around 77%, with deaths occurring after the third day post-infusion. The administration of SS31 significantly increased the survival rate in Ang II-infused ApoE$^{-/-}$ mice, from 77% to 95%, whereas SS20, a structurally related tetrapeptide without antioxidant properties, had no effect on survival rate (Figure 1a). To follow-up AAA progression during the in vivo study, aortic diameter was monitored by ultrasonography at 0, 3, 7, 14 and 28 days after Ang II infusion (Figure 1b). Interestingly, SS31 attenuated the increase in aortic diameter in response to Ang II infusion from the first week of treatment until Day 28 and remained significantly different compared with untreated Ang II-infused ApoE$^{-/-}$ mice from Day 7, in contrast to SS20-treated animals (Figure 1b–d). Accordingly, the incidence of AAA was greatly reduced in Ang II-challenged mice treated with SS31, unlike SS20 (Figure 1e). Furthermore, only SS31 reduced the percentage of animals affected by the

**FIGURE 1** Mitochondrial stress inhibition with SS31 reduces aortic diameter in Ang II-infused ApoE$^{-/-}$ mice. ApoE$^{-/-}$mice were infused with either saline (n = 15) or Ang II (n = 27) and treated with SS31 (n = 18) or SS20 (n = 18). (a) Graph showing the survival rates of each group of animals (n = 15–27). Data are expressed as mean ± SEM. $P < 0.05$: * versus saline at 28 days; $ versus SS20 + Ang II or Ang II at 28 days (Kaplan–Meier analysis). (b) Time-course analysis of abdominal aortic diameters (mm) evaluated by ultrasonography at 0, 3, 7, 14, 21 and 28 days of Ang II infusion in each experimental group (n = 15–22). Data are expressed as mean ± SEM. $P < 0.05$: * versus saline at 28 days; $ versus SS20 + Ang II at 28 days and # versus Ang II (two-way ANOVA with post hoc Bonferroni's test). (c) Maximal suprarenal abdominal aortic diameter (in mm) measured from transverse ultrasound images at Day 28 post-infusion (n = 15–22). Data are expressed as mean ± SEM. $^{*}P < 0.05$ versus saline; $^{\#}P < 0.05$ versus Ang II (one-way ANOVA with post hoc Bonferroni's test); $^{\$}P < 0.05$ versus SS20. (d) Representative images of fixed aortas from males of the different groups. (e) Histogram representing the incidence of abdominal aortic aneurysm (AAA) in percentage ($\chi^2$ test). $P < 0.05$: * versus saline; $ versus Ang II or SS20 + Ang II (f) Representative aortic sections stained with Masson's trichrome (scale bars: 200 μm). (g) Orcein staining showing the elastic fibres morphology (scale bars: 100 μm). Arrows indicate elastic fibre ruptures, and the histogram shows the quantification of the number of ruptures of elastic fibres (below). Results are expressed as mean ± SEM from n = 5. $P < 0.05$: * versus saline; # versus Ang II; $ versus SS20 (one-way ANOVA with Tukey's multiple comparisons test). (h, i) *Mmp2* and *Mmp9* mRNA levels analysed by real-time PCR and normalized to *Gapdh*. Results are expressed as mean ± SEM from n = 10–14. $P < 0.05$: * versus saline; # versus Ang II; $ versus SS20 (one-way ANOVA with Tukey's multiple comparisons test).

**TABLE 1** Blood pressure values at Day 28 of Ang II infusion.

| Arterial pressure (mmHg) | Systolic | Diastolic | MAP |
|---|---|---|---|
| ApoE$^{-/-}$ + saline (n = 13) | 100.8 ± 0.7 | 70.8 ± 1.9 | 81.6 ± 1.4 |
| ApoE$^{-/-}$ + Ang II (n = 16) | 136.10 ± 1.1* | 103.38 ± 3.1* | 114.55 ± 2.5* |
| ApoE$^{-/-}$Ang II + SS31 (n = 18) | 131.6 ± 3.1* | 98.95 ± 2.6* | 111.1 ± 3.0* |
| ApoE$^{-/-}$Ang II + SS20 (n = 16) | 140.4 ± 2.76* | 105.7 ± 3.1* | 119.1 ± 3.0* |
| ApoE$^{-/-}$Ang II + PBA (n = 13) | 118.5 ± 3.9*# | 92.2 ± 4.2* | 101.9 ± 4.6* |
| ApoE$^{-/-}$Ang II + TUDCA (n = 14) | 121.09 ± 2.8*# | 94.35 ± 4.3* | 102.9 ± 3.62* |
| ApoE$^{-/-}$/CHOP$^{-/-}$ + saline (n = 7) | 98.82 ± 2.8# | 74.55 ± 3.2*# | 82.29 ± 2.9# |
| ApoE$^{-/-}$/CHOP$^{-/-}$ + Ang II (n = 11) | 122.57 ± 3.0*# | 88.62 ± 2.1*# | 99.53 ± 2.1*# |
| ApoE$^{-/-}$/CHOP$^{+/+}$ + Ang II (n = 7) | 138.01 ± 4.9* | 110.01 ± 4.8* | 118.98 ± 4.2* |

*Note*: Blood pressure values are expressed as mean ± SEM. The experimental group and the number of animals are indicated in the left column.
Abbreviations: Ang II, angiotensin II; ApoE, apolipoprotein-E; CHOP, C/EBP homologous protein; MAP, mean arterial pressure; PBA, 4-phenylbutyrate; SS, Szeto-Schiller; TUDCA, tauroursodeoxycholic acid.
*$P < 0.05$ versus saline.
#$P < 0.05$ versus Ang II (one-way ANOVA).

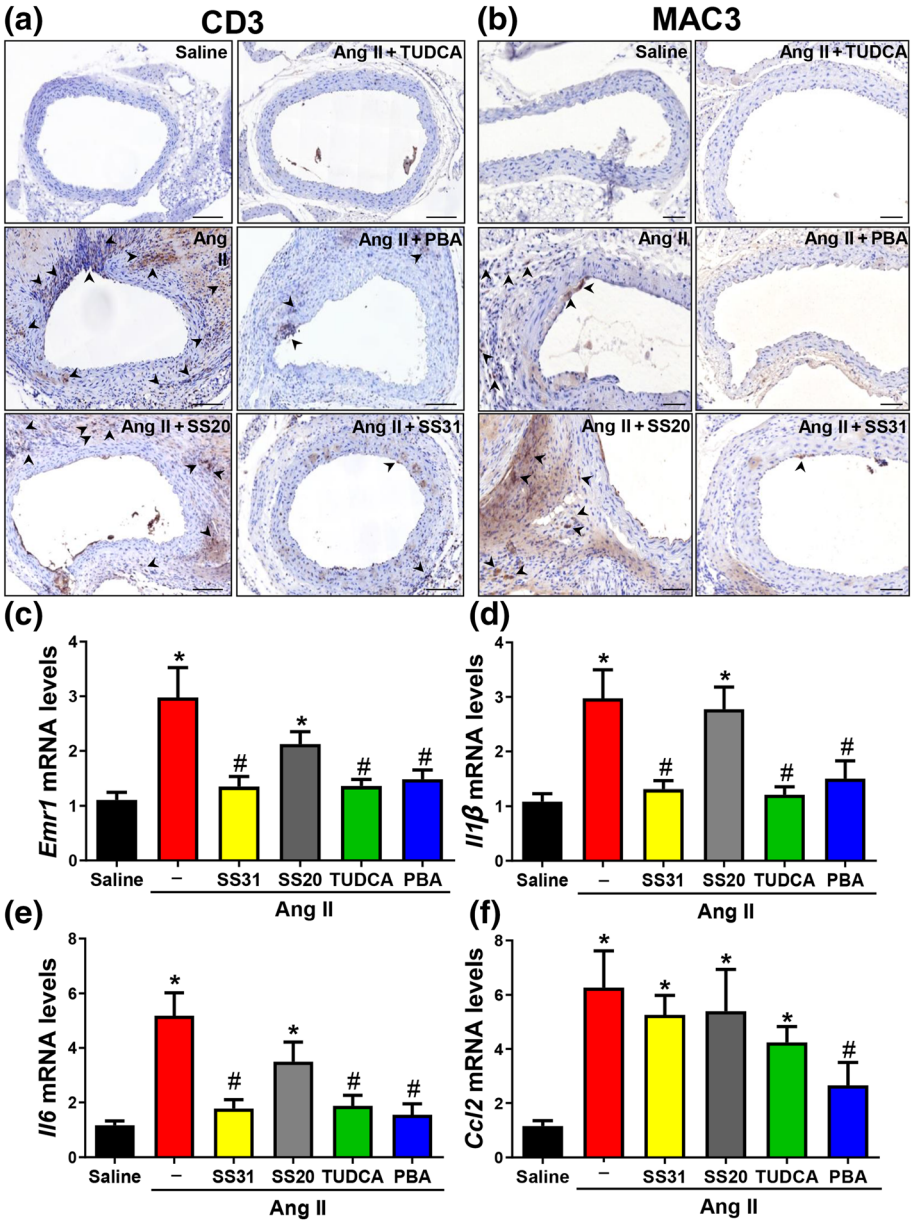


**FIGURE 2** Immune cell infiltration is reduced by the administration of SS31 and both endoplasmic reticulum stress inhibitors in abdominal aorta from Ang II-infused ApoE$^{-/-}$mice. ApoE$^{-/-}$ mice were infused with either saline or Ang II treated or not with SS31, SS20, TUDCA or PBA. (a, b) Representative images corresponding to lymphocytes (CD3, left panels) and macrophages (Mac-3, right panels) infiltration analysed by immunohistochemistry. Arrows indicate positive cells for each marker (n = 5). Scale bars: 50 µm. (c–f) The abdominal aortic expression of *Emr1*, *Il1β*, *Il6* and *Ccl2* was evaluated by real-time PCR and normalized to *Gapdh* mRNA levels (n = 10–15). Values shown are mean ± SEM. $P < 0.05$: * versus saline; # versus Ang II (one-way ANOVA with post hoc Bonferroni's test).

most severe forms of AAA, whereas Ang II-infused mice untreated or treated with SS20 developed highly complex aneurysms (Figure S1A). None of the peptides affected the augment in blood pressure triggered by Ang II (Table 1).

### 3.2 | SS31 decreases vascular remodelling, ROS and inflammation and modulates ER stress in abdominal aorta

Histological analyses showed that in ApoE$^{-/-}$ mice, the Ang II-induced compensatory increase in collagen deposition was attenuated exclusively by SS31 (Figure 1f), which also limited the disorganization and rupture of elastic fibres (Figure 1g). In agreement, SS31 significantly ameliorated the increased aortic expression of MMP2 and MMP9 induced by Ang II, in contrast to SS20 (Figure 1h,i). The massive infiltration of immune cells in the aortic wall is a hallmark of the aneurysmal process (Potteaux & Tedgui, 2015; Shimizu et al., 2006). SS31 reduced the vascular content of macrophages (MAC3 positive) and T-cells (CD3 positive) (Figure 2a,b) and prevented the Ang II-induced expression of *Emr1*, *Il1β* and *Il6* (Figure 2c–e).

Plasmatic ROS levels were significantly decreased in hypertensive mice receiving SS31 compared with those treated with SS20 (Figure 3a). Furthermore, SS31, but not SS20, ameliorated the striking oxidative DNA damage induced by Ang II, as evidenced by the reduction in the aortic staining for 8-oxo-dG (Figure 3b). Additionally, SS31 restored the abnormal expression of the cytochrome

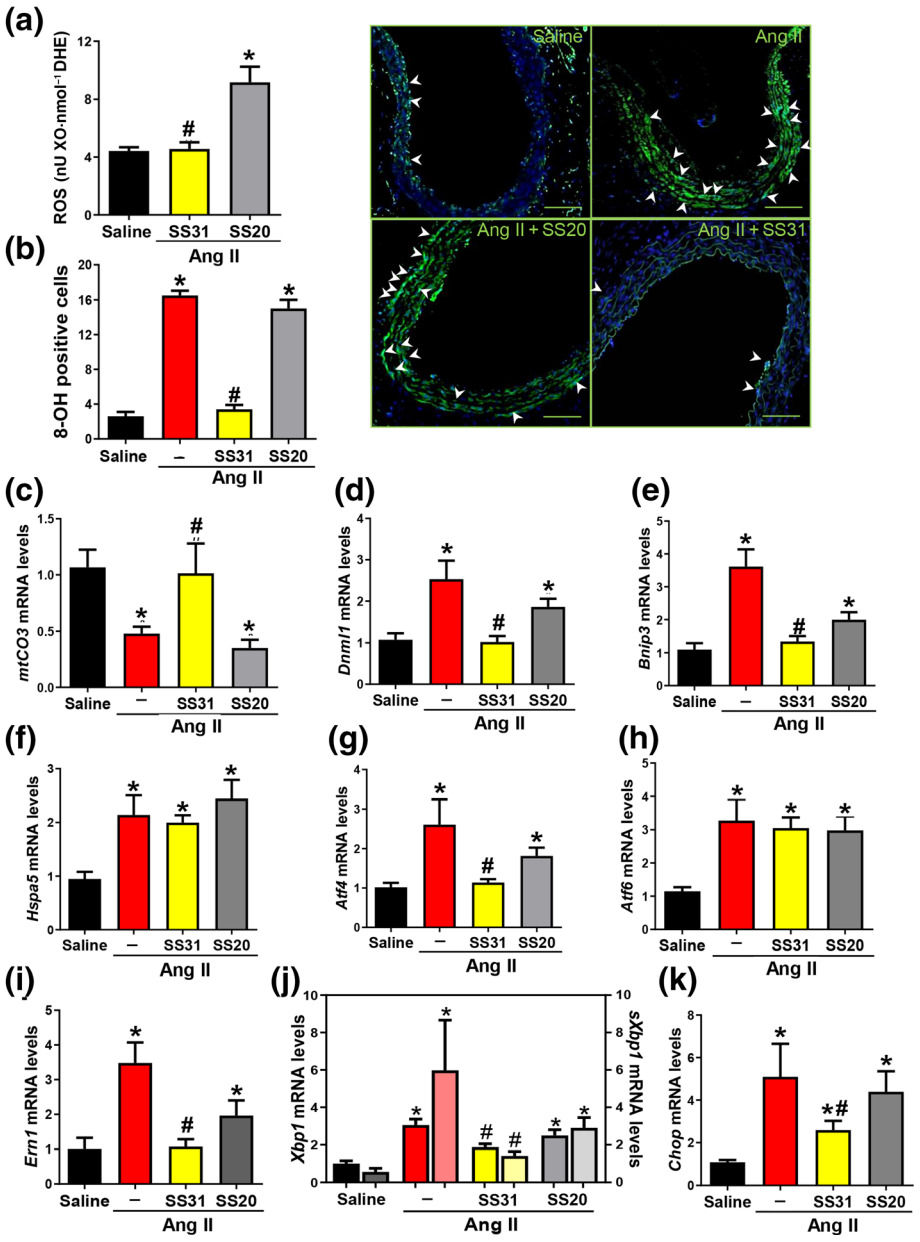


**FIGURE 3** Oxidative stress and expression of mitochondrial dysfunction and endoplasmic reticulum stress markers in the abdominal aorta from Ang II-infused ApoE$^{-/-}$ mice treated with SS31. ApoE$^{-/-}$ mice were infused with either saline (Sal) or Ang II. Ang II-infused ApoE$^{-/-}$ mice were untreated or treated with SS31 or SS20. (a) Quantification of ROS plasma levels in either saline or Ang II infused mice treated with SS20 or SS31 (n = 5–8). Results are expressed as mean ± SEM. $^{*}P < 0.01$ versus saline; $^{\#}P < 0.05$ versus Ang II (one-way ANOVA with Tukey's multiple comparisons test). (b) Histogram showing number of positive cells for 8-oxo-dG (8-OH) immunostaining and representative images of immunostaining assays performed in abdominal aorta sections targeting 8-oxo-dG (n = 5–6). Positive stained cells/nuclei are indicated with arrowheads (bars: 50 μm). Results are expressed as mean ± SEM. $^{*}P < 0.01$ versus saline; $^{\#}P < 0.05$ versus Ang II (one-way ANOVA with Tukey's multiple comparisons test). (c–e) Abdominal aortic expression of *mtCo3*, *Dnml1* and *Bnip3* was evaluated by real-time PCR (n = 10–15). (f–k) Quantitative analysis of the mRNA levels of *Hspa5*, *Atf4*, *Atf6*, *Ern1*, *Xbp1*, *sXbp1* and *Chop* (n = 10–15). Values, normalized to *Gapdh* expression, are shown as mean ± SEM. $P < 0.05$: * versus saline; # versus Ang II (one-way ANOVA with Tukey's multiple comparisons test/Kruskal–Wallis test).

c oxidase subunit III (*Cox3*), a mitochondrial biogenesis indicator, and of two mitophagy markers: the dinamin-related protein 1 (*Dnm1l*) and the BCL2/adenovirus E1B 19-kDa protein-interacting protein 3 (*Bnip3*) that were induced by Ang II, whereas SS20 had no effect (Figure 3g–i). More interestingly, SS31 decreased the Ang II-induced expression of specific ER stress markers involved in the *Atf4* and *Ern1/Xbp1* axis (Figures 3c–f and S4), although ATF4 protein levels were not significantly normalized by SS31 (data not shown).

### 3.3 | ER stress inhibition in Ang II-infused ApoE$^{-/-}$ mice prevents AAA through an attenuation of vascular remodelling and inflammation

Similarly to what we previously reported in human AAA (Navas-Madroñal et al., 2019), the expression of ER stress markers was increased in the abdominal aorta of Ang II-infused ApoE$^{-/-}$mice as observed in the time-course analysis of *Hspa5*, *Atf4*, *Atf6*, *Ern1* and *Chop* expression in response to Ang II infusion (Figure S2). As the beneficial effects of SS31 on aneurysm development are coupled to a reduction of vascular ER stress, we aimed to determine whether the attenuation of AAA by ER stress inhibitors resembled that observed in SS31-treated mice.

Ang II-infused ApoE$^{-/-}$ mice were treated with two well-known ER stress inhibitors: TUDCA and PBA, which differentially modulated the Ang II-induced up-regulation of ER stress markers in ApoE$^{-/-}$ mice (Figures S3 and S4). TUDCA decreased the expression of these markers, whereas PBA only effectively attenuated that of the *Atf6* and *Ern1/Xbp1* axis, in contrast to SS31. Of note, TUDCA prevented the decrease of the mitochondrial biogenesis marker *Cox3*, whereas neither TUDCA nor PBA normalized the altered expression of mitophagy markers (Figure S3). The inhibition of ER stress with either PBA or TUDCA significantly reduced SBP but did not alter biochemical parameters (Tables 1 and S1).

In agreement with the response induced by SS31, TUDCA significantly improved the survival rate which rose above 94%, but PBA only delayed the occurrence of deathly events (Figure 4a). ER stress inhibitors slowed down the progressive increase of aortic dilation induced by Ang II from the first week of treatment until Day 28 and remained significantly different compared with untreated Ang II-infused ApoE$^{-/-}$ mice from Day 7 of Ang II infusion, a temporal profile analogous to that found in SS31-treated mice (Figure 4b).

At the end of the study, a significant attenuation of aortic diameter exerted by these drugs was manifest (Figure 4c–e). The administration of TUDCA and PBA reduced the incidence of AAA to 20% (Figure 4f) and limited the severity of aneurysmal lesions (Figure S1).

ER stress inhibitors attenuated Ang II-induced vascular remodelling, improving overall aorta morphology. Likewise, both chemicals preserved the vessel wall integrity, as did SS31, by reducing the compensatory synthesis and deposition of collagen fibres observed in Ang II-infused ApoE$^{-/-}$mice and by reducing the disruption of elastin fibres (Figure 5a–c). Accordingly, the induction of MMP9 and MMP2 expression and activity was significantly ameliorated by TUDCA, whereas PBA only reduced that of MMP9 (Figure 5d–g). Additionally, both ER stress inhibitors limited the substantial inflammatory infiltration induced by Ang II (Figure 2a,b) and attenuated the expression of *Emr1*, *Il1β* and *Il6*, whereas *Ccl2* expression, which remained unaltered in SS31- and TUDCA-treated mice, was significantly reduced by PBA (Figure 2c–f).

### 3.4 | CHOP deficiency reduces Ang II-induced AAA formation in ApoE$^{-/-}$ mice

Due to the striking increase of *Chop* expression in aneurysmal aortas from patients with AAA (Navas-Madroñal et al., 2019; Qin et al., 2017) and Ang II-infused ApoE$^{-/-}$ mice (Figure S2) and to further explore the mechanisms by which ER stress inhibition prevented the formation and progression of AAA, we studied whether or not knockdown of *Chop* influenced aneurysm formation. For this purpose, ApoE$^{-/-}$/CHOP$^{-/-}$ mice and their corresponding ApoE$^{-/-}$/CHOP$^{+/+}$ littermates were challenged with either Ang II or saline solution for 28 days. The lack of CHOP in ApoE$^{-/-}$ mice neither significantly improved the survival rate (2 of 13 Ang II-infused ApoE$^{-/-}$/CHOP$^{-/-}$ died of aortic rupture vs. 3 of 16 in ApoE$^{-/-}$/CHOP$^{+/+}$) nor delayed the occurrence of fatal events (Figure 6a). No spontaneous AAA was observed in saline-infused ApoE$^{-/-}$/CHOP$^{-/-}$ mice. However, *Chop* deficiency significantly prevented the Ang II-induced abdominal aortic dilation, as shown by ultrasound monitorization (Figure 6b–d), and reduced the incidence of aneurysm (to a 36%) in comparison with Ang II-infused ApoE$^{-/-}$ mice expressing *Chop* (86%) (Figure 6e). Despite the improvement in aneurysm development, the Ang II-induced expression of inflammatory markers was maintained in *Chop*-deficient mice (Figure S5A). Further, after Ang II infusion, CHOP-deficient mice exhibited a significant reduction in blood pressure like that evoked by TUDCA and PBA (Table 1).

Finally, the up-regulation of ER stress markers by Ang II in AAA was not affected by *Chop* knockdown, whereas, as expected, *Chop* mRNA levels were undetectable in the double KO mice (Figure S5B).

### 3.5 | Hypertensive cardiac hypertrophy and dysfunction were improved by SS31 and ER stress inhibition

The expression of several ER stress markers such as *Hspa5*, *Atf4* and *Chop* was increased in the heart of Ang II-infused ApoE$^{-/-}$mice (Figure S6). SS31, PBA and TUDCA limited the exacerbated expression of *Hspa5*, *Atf4* and *Chop* in the heart (Figure S6A–D). Hence, we determined whether SS31 and ER stress inhibitors could impact on cardiac dysfunction and hypertrophic remodelling induced by Ang II

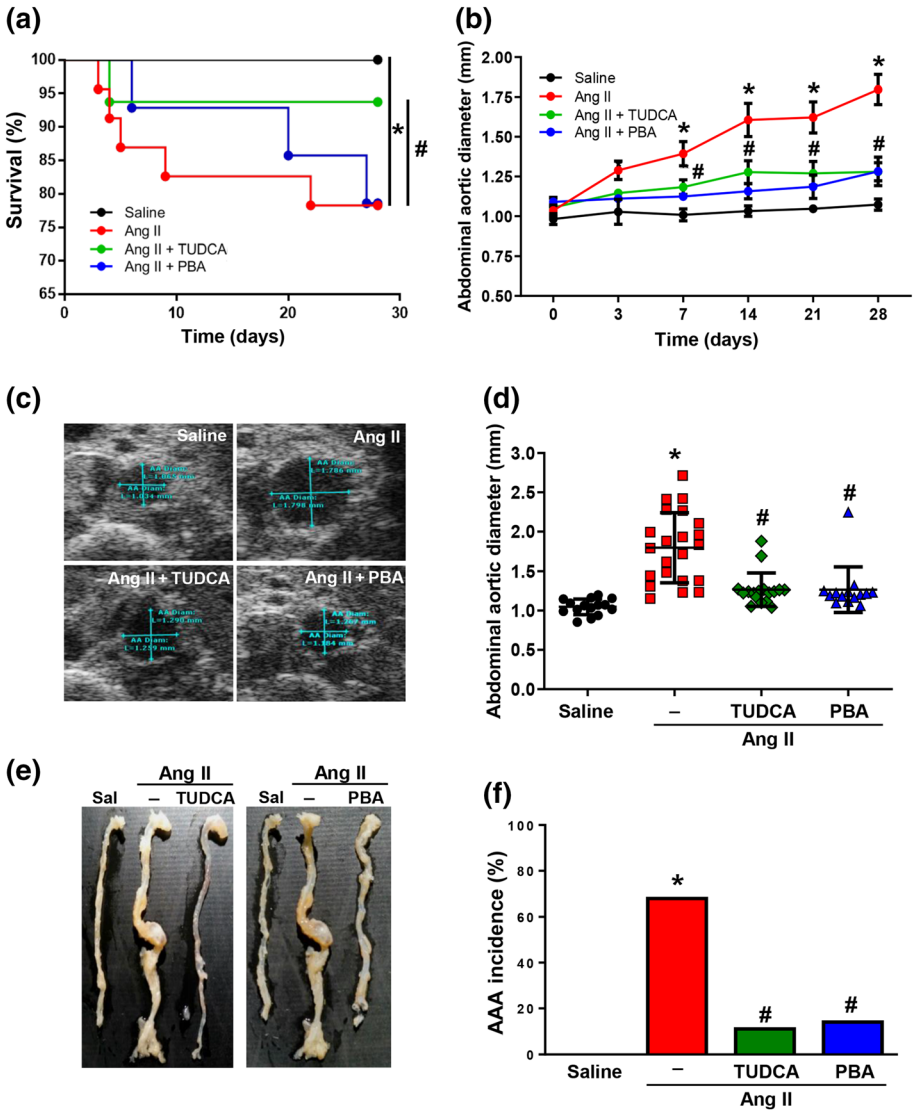


**FIGURE 4** The progression of abdominal aortic aneurysm (AAA) is reduced during the time of infusion with Ang II by the administration of endoplasmic reticulum stress inhibitors. ApoE$^{-/-}$ mice were infused with either saline (Sal) or Ang II and were treated or not with TUDCA or PBA. (a) Graph showing the survival rates of each group of animals (n = 15–27). All animals from saline group survived until the end of the study. $P < 0.05$: * versus saline at 28 days; # versus Ang II at 28 days (Kaplan–Meier analysis). (b) Time-course analysis of abdominal aortic diameters (mm) evaluated by ultrasonography at 0, 3, 7, 14, 21 and 28 days of Ang II infusion in all group of animals (n = 15–22). Data are expressed as mean ± SEM. $P < 0.05$: * versus saline at 7, 14, 21 and 28 days; # versus Ang II at 14, 21 and 28 days (two-way ANOVA/Bonferroni's test). (c) Representative high-frequency ultrasound frames of abdominal aortas from all groups. (d) Transverse (top) images were taken at the level of the suprarenal aorta and maximal suprarenal abdominal aortic diameter (in mm) measured from transverse ultrasound images at Day 28 post-infusion (n = 15–22). Data are expressed as mean ± SEM. $P < 0.05$: * versus saline; # versus Ang II (one-way ANOVA post hoc Bonferroni's test). (e) Representative images of fixed aortas from males of the four groups. (f) Histogram representing the incidence of AAA in percentage of mice of each group. $P < 0.05$: * versus saline; # versus Ang II (control [saline] animals are the same than those in Figure 1; $\chi^2$ test).

infusion in ApoE$^{-/-}$ mice. Interestingly, the compensatory increase in EF induced by Ang II-infusion was abolished by either SS31 or TUDCA. Heart rate, cardiac output and stroke volume were not altered by Ang II infusion or pharmacological interventions. In turn, the Ang II-induced hypertrophic response was ameliorated by SS31 and TUDCA, which reduced LV mass and thickness (Table 2). These data suggested that concentric remodelling in response to Ang II was partially prevented by SS31 and TUDCA, whereas PBA had no impact on Ang II-induced cardiac dysfunction and remodelling. As hypertrophic markers, whereas *Anp* mRNA levels were decreased by SS31 and TUDCA, those of *Myh7* were only attenuated by ER stress inhibition (Figure S6E,F).

Echocardiographic analysis of ApoE$^{-/-}$/CHOP$^{-/-}$ mice revealed that the lack of *Chop* prevented the hypertrophic effects of Ang II infusion, normalizing systolic function parameters to those found in saline-infused ApoE$^{-/-}$/CHOP$^{-/-}$ mice and significantly reducing

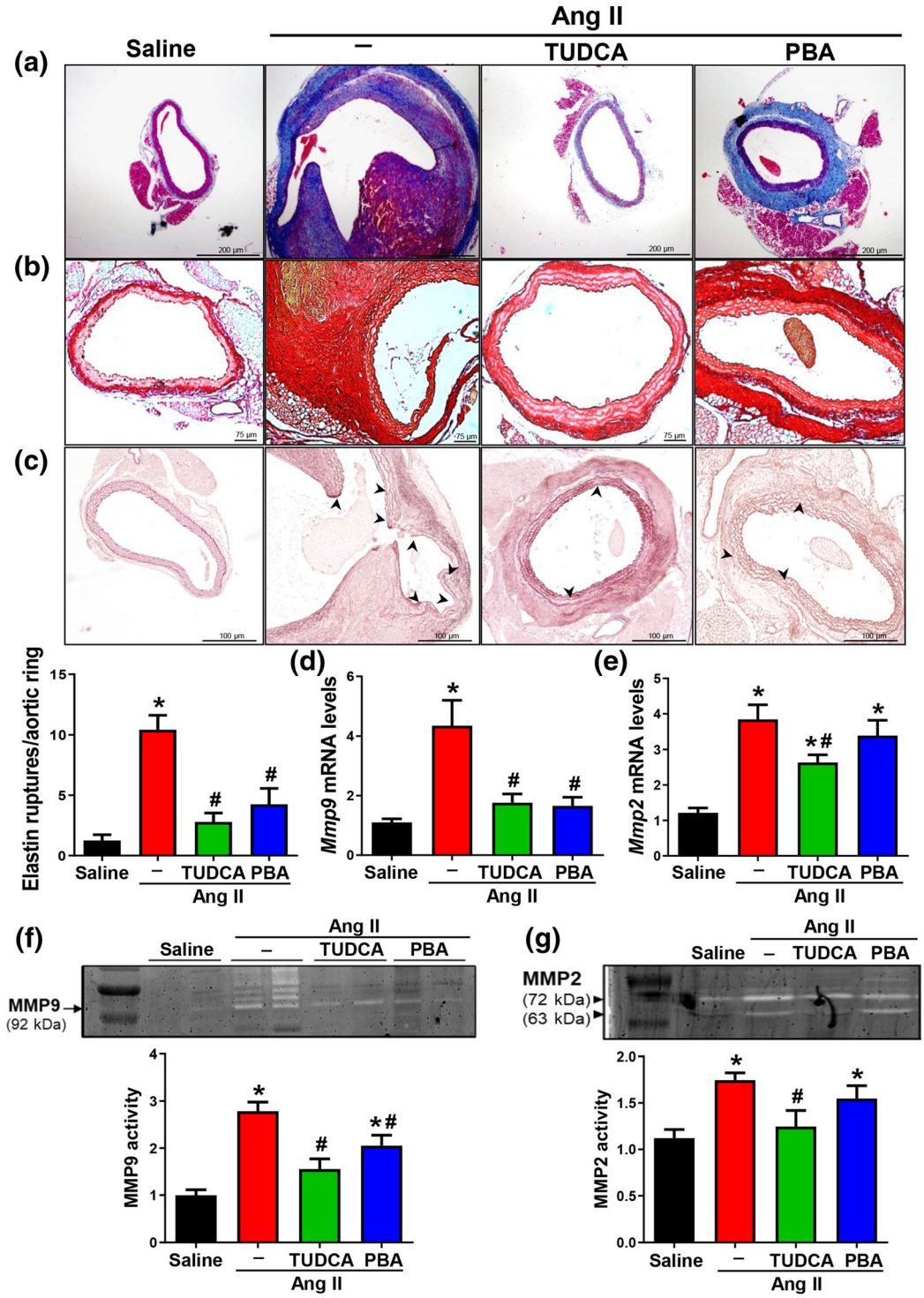


**FIGURE 5** Extracellular matrix disorganization and MMP expression/activity were reduced by endoplasmic reticulum stress inhibitors in the abdominal aorta from Ang II-infused ApoE$^{-/-}$ mice. ApoE$^{-/-}$ mice were infused with either saline or Ang II. Ang II-infused ApoE$^{-/-}$ mice were untreated or treated with PBA or TUDCA. (a) Representative aortic sections stained with Masson's trichrome captured with 4× objective as indicated (scale bars: 200 µm). (b) Representative aortic sections stained with sirius red (scale bars: 75 µm). (c) Orcein staining showing the elastic fibres morphology (scale bars: 100 µm). Arrows indicate elastic fibres ruptures, and histogram shows the quantification of the number of ruptures. Results are expressed as mean ± SEM from n = 5. $P < 0.05$: * versus saline; # versus Ang II (Kruskal–Wallis test). (d, e) *Mmp9* and *Mmp2* mRNA levels are analysed by real-time PCR and normalized to GAPDH (n = 10–15). Results are shown as the mean ± SEM. $P < 0.05$: * versus saline; # versus Ang II (one-way ANOVA post hoc Bonferroni's test). (f, g) Representative gelatin gel zymography to detect MMP zymogens (pro-MMP) and active forms of MMP9 and MMP2 in protein extracts of murine abdominal aortas from each group. Histograms represent the densitometric quantification of active forms for both MMPs (n = 8–10). Results are shown as the mean ± SEM. $P < 0.05$: * versus saline; # versus Ang II (one-way ANOVA post hoc Bonferroni's test).

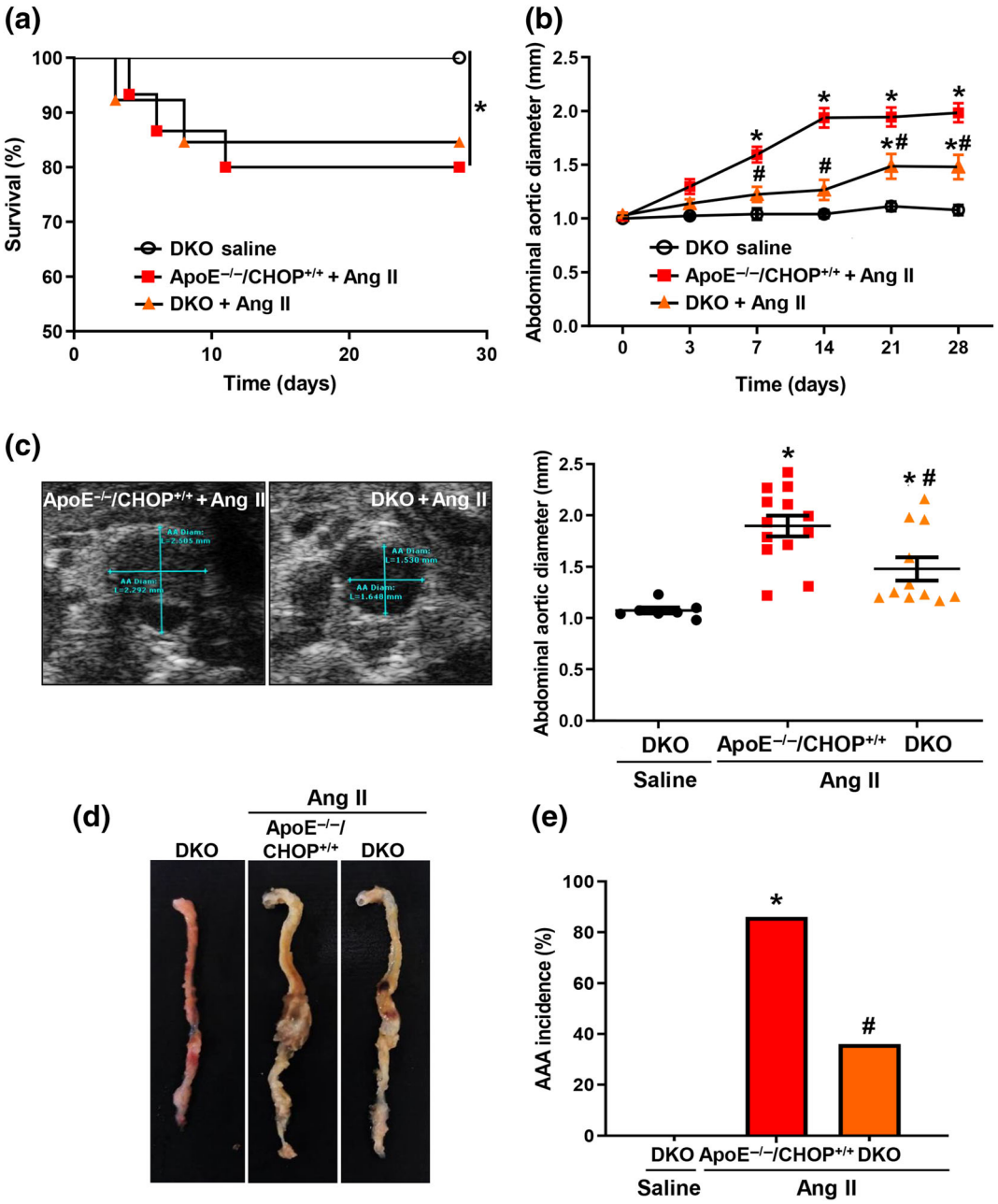


**FIGURE 6** The progression of abdominal aortic aneurysm (AAA) was reduced in ApoE$^{-/-}$/CHOP$^{-/-}$ mice. ApoE$^{-/-}$/CHOP$^{-/-}$ (DKO) males were infused with saline (n = 7) or Ang II (n = 13) whereas their Ang II-infused ApoE$^{-/-}$/CHOP$^{+/+}$ littermates were infused with Ang II (n = 16). (a) Graph showing the survival rates of each experimental group (n = 7–16). All saline-infused animals survived until the end of the study. *$P$ < 0.05 versus saline at 28 days (Kaplan–Meier analysis). (b) Time-course analysis of abdominal aortic diameters (mm) evaluated by ultrasonography at 0, 3, 7, 14, 21 and 28 days of either Ang II or saline infusion (n = 7–13). Data are expressed as mean ± SEM. $P$ < 0.05: * versus DKO saline at 7, 14, 21 and 28 days; # versus ApoE$^{-/-}$/CHOP$^{+/+}$ + Ang II at 7, 14, 21 and 28 days (two-way ANOVA/Bonferroni's test). (c) Representative high-frequency ultrasound frames of abdominal aortas from Ang II-infused ApoE$^{-/-}$/CHOP$^{+/+}$ and DKO mice. Images (left) were taken at the level of the suprarenal aorta. The maximal suprarenal abdominal aortic diameter (in mm) at Day 28 post-infusion, measured from transverse ultrasound images, is indicated and the quantitative analysis is represented on the right (n = 7–13). Data are expressed as mean ± SEM. $P$ < 0.05: * versus DKO saline; # versus ApoE$^{-/-}$/CHOP$^{+/+}$ + Ang II (one-way ANOVA post hoc Bonferroni's test). (d) Representative images of fixed aortas from DKO and Ang II-infused ApoE$^{-/-}$/CHOP$^{+/+}$ males. (e) Histogram representing the incidence of AAA in percentage. $P$ < 0.05: * versus DKO saline; # versus ApoE$^{-/-}$/CHOP$^{+/+}$ + Ang II ($\chi^2$ test).

LV mass (Table 3). Additionally, the increased E/A ratio found in Ang II-infused ApoE$^{-/-}$ mice, indicative of an early diastolic dysfunction, was significantly attenuated in mice treated with either SS31 or SS20 and in those receiving TUDCA. IVRT and MVET values remained unchanged in all the experimental groups (Table S2).

**TABLE 2** Systolic function parameters in all groups of ApoE$^{-/-}$ mice.

| Parameters | Saline (n = 12) | Ang II (n = 16) | SS31 (n = 17) | SS20 (n = 16) | TUDCA (n = 12) | PBA (n = 10) |
|---|---|---|---|---|---|---|
| LVAWd (mm) | 0.97 ± 0.04 | 1.29 ± 0.03* | 1.12 ± 0.15 | 1.22 ± 0.05 | 1.15 ± 0.05 | 1.32 ± 0.06* |
| LVAWs (mm) | 1.37 ± 0.06 | 1.85 ± 0.04* | 1.58 ± 0.04# | 1.76 ± 0.09* | 1.71 ± 0.06* | 1.85 ± 0.07* |
| IVSd (mm) | 1.08 ± 0.08 | 1.23 ± 0.03 | 1.14 ± 0.05 | 1.24 ± 0.03 | 1.13 ± 0.04 | 1.28 ± 0.05 |
| IVSs (mm) | 1.45 ± 0.08 | 1.79 ± 0.02* | 1.57 ± 0.05# | 1.77 ± 0.06 | 1.65 ± 0.07 | 1.84 ± 0.06* |
| LVIDd (mm) | 3.52 ± 0.11 | 3.11 ± 0.10* | 3.51 ± 0.08# | 3.3 ± 0.1 | 3.28 ± 0.11 | 2.99 ± 0.12* |
| LVIDs (mm) | 2.42 ± 0.12 | 2.03 ± 0.11* | 2.48 ± 0.09# | 2.19 ± 0.13 | 2.25 ± 0.10 | 1.84 ± 0.12* |
| LVPWd (mm) | 0.88 ± 0.04 | 1.20 ± 0.05* | 1.13 ± 0.06 | 1.16 ± 0.05 | 1.16 ± 0.05 | 1.24 ± 0.06* |
| LVPWs (mm) | 1.30 ± 0.06 | 1.63 ± 0.07* | 1.55 ± 0.04 | 1.55 ± 0.06 | 1.55 ± 0.06* | 1.70 ± 0.07* |
| EF (%) | 61.42 ± 1.05 | 73.07 ± 1.93* | 61.76 ± 1.95# | 65.60 ± 2.06 | 64.33 ± 2.36# | 72.34 ± 1.53* |
| FS (%) | 32.83 ± 2.20 | 40.27 ± 1.87* | 33.40 ± 1.35# | 34.94 ± 1.67 | 35.29 ± 1.98 | 41.19 ± 1.28* |
| LV mass (mg) | 92.27 ± 3.12 | 133.09 ± 2.49* | 114.12 ± 3.68*# | 122.21 ± 5.13* | 117.97 ± 4.39*# | 119.78 ± 5.05* |
| HR (bpm) | 396.86 ± 11.78 | 393.09 ± 10.75 | 424.00 ± 10.09 | 424.69 ± 6.85 | 374.43 ± 11.97 | 397 ± 11.96 |
| Stroke volume | 30.83 ± 1.53 | 29.41 ± 1.50 | 28.91 ± 1.62 | 28.62 ± 1.74 | 27.40 ± 1.95 | 24.40 ± 1.90 |
| Cardiac output | 12.19 ± 0.63 | 11.30 ± 0.59 | 11.64 ± 0.73 | 11.98 ± 0.73 | 9.96 ± 0.90 | 9.43 ± 0.85 |

*Note*: Results are expressed as mean ± SEM.

Abbreviations: Ang II, angiotensin II; ApoE, apolipoprotein-E; bpm, beats per minute; EF, ejection fraction; FS, fractional shortening; HR, heart rate; IVS, interventricular septum; LV, left ventricular; LVAW, LV anterior wall thickness; LVID, LV internal diameter; LVPW, LV posterior wall thickness; PBA, 4-phenylbutyrate; SS, Szeto-Schiller; TUDCA, tauroursodeoxycholic acid.

*$P$ < 0.05 versus saline.

#$P$ < 0.05 versus Ang II group (one-way ANOVA).

## 4 | DISCUSSION

AAAs and their rupture significantly contribute to morbidity and mortality in elderly people. Unfortunately, therapeutic strategies in AAA are restricted to either open or endovascular surgical repair of aneurysms under a high risk of rupture, and there are still no effective pharmacological drugs that limit AAA progression and rupture. Despite efforts having been made to improve the outcome of these patients, surgical repair is related to significant short-term and long-term morbidity and mortality (Golledge, 2019; Klink et al., 2011; Ulug et al., 2020). The search for therapies that improve the management of patients with AAA remains a challenge that requires a deeper understanding of the mechanisms involved in the onset, growth and rupture of aortic aneurysms.

Despite the outstanding progress on the pathophysiological role of mitochondrial oxidative stress and ER stress in cardiovascular pathologies, the knowledge about their involvement in AAA development is incomplete (Dikalova et al., 2010; Guzik et al., 2013; Usui et al., 2015). Mitochondrial dysfunction and ER stress are closely associated, and their deleterious crosstalk promotes the excessive generation of mitochondrial ROS, which are cytotoxic and induce organ dysfunction and injury. Specifically, mitochondrial dysfunction is a hallmark of human AAA, as previously reported (Navas-Madroñal et al., 2019); however, its contribution to aneurysmal disease is unclear. In agreement with human data, our study reveals a disturbance of mitochondrial function in the most common experimental model of this disease, the Ang II-infused ApoE$^{-/-}$mice.

Notably, we found that the increase in aortic diameter and high incidence of AAA triggered by Ang II in ApoE$^{-/-}$ mice were strikingly ameliorated by SS31, which virtually suppressed mortality, in contrast to SS20, a structurally related mitochondria-targeted peptide without antioxidant properties (Szeto, 2008; Zhao et al., 2004), used as a control peptide in our studies. SS31 also preserved elastic fibre integrity and aortic wall structure, reducing MMP expression and vascular inflammation. This peptide improved mitochondrial biogenesis and integrity through the restoration of the expression of mt-CO3 and the reduction of Dnml1 and Bnip3, which play an important role in the regulation of mitochondrial division and maintenance of mitochondrial structures participating in mitochondrial fission and mitophagy to preserve mitochondria quality (Kleele et al., 2021). Interestingly, these beneficial effects in response to SS31 were associated with a reduction in both circulating oxidative stress and aortic ROS-dependent DNA damage, in agreement with the ability of this peptide to attenuate the production of toxic mitochondrial ROS reported in other pathological scenarios (Kloner et al., 2015). Because excessive vascular oxidative stress is a key feature underlying vascular degeneration in AAA (Emeto et al., 2016), targeting mitochondrial oxidative stress by SS31 could be particularly useful for the treatment of AAA, as well as suggested for other vascular disorders (Cai et al., 2018; Lu et al., 2016; M. Zhang et al., 2017; J. Zhang, Wang, et al., 2021).

It has been previously reported that SS31 reduces mitochondrial ROS and ER stress in vitro in leukocytes from patients with type 2 diabetes mellitus (Escribano-López et al., 2019). Similarly, and beyond its favourable response on ROS production, SS31 also ameliorated the enhanced expression of ER markers, mainly those involved in the

**TABLE 3** Systolic and diastolic function parameters in double KO males in comparison with their ApoE$^{-/-}$/CHOP$^{+/+}$ littermates in response to Ang II.

| Parameters | ApoE$^{-/-}$ Saline (n = 10) | Double KO Saline (n = 6) | ApoE$^{-/-}$/CHOP$^{+/+}$ Ang II (n = 9) | Double KO Ang II (n = 11) |
|---|---|---|---|---|
| LVAWd (mm) | 0.95 ± 0.04 | 0.97 ± 0.02 | 1.27 ± 0.04* | 0.99 ± 0.07# |
| LVAWs (mm) | 1.35 ± 0.07 | 1.46 ± 0.06 | 1.85 ± 0.05* | 1.39 ± 0.07# |
| IVSd (mm) | 1.08 ± 0.09 | 0.92 ± 0.08 | 1.21 ± 0.04 | 0.88 ± 0.03# |
| IVSs (mm) | 1.57 ± 0.08 | 1.44 ± 0.11 | 1.76 ± 0.04* | 1.28 ± 0.06# |
| LVIDd (mm) | 3.55 ± 0.11 | 3.62 ± 0.15 | 3.22 ± 0.14* | 3.54 ± 0.10 |
| LVIDs (mm) | 2.50 ± 0.11 | 2.44 ± 0.19 | 2.03 ± 0.17* | 2.44 ± 0.13# |
| LVPWd (mm) | 0.88 ± 0.04 | 0.87 ± 0.03 | 1.15 ± 0.09 | 1.00 ± 0.07 |
| LVPWs (mm) | 1.30 ± 0.06 | 1.32 ± 0.09 | 1.63 ± 0.09* | 1.43 ± 0.07 |
| EF (%) | 61.56 ± 3.45 | 64.04 ± 4.19 | 72.88 ± 2.64* | 59.53 ± 2.25# |
| FS (%) | 32.98 ± 2.40 | 34.64 ± 3.23 | 39.32 ± 2.61 | 31.16 ± 1.56# |
| LV mass (mg) | 92.11 ± 3.42 | 93.29 ± 5.95 | 132.24 ± 3.35* | 102.09 ± 6.54# |
| HR (bpm) | 394.08 ± 12.85 | 384.25 ± 9.00 | 393.09 ± 14.33 | 387.25 ± 6.30 |
| Stroke volume | 30.68 ± 1.67 | 36.22 ± 4.02 | 29.41 ± 1.99 | 29.92 ± 3.23 |
| Cardiac output | 11.56 ± 0.69 | 11.65 ± 2.12 | 11.30 ± 0.78 | 11.13 ± 0.91 |
| AET (ms) | 52.69 ± 1.77 | 50.99 ± 2.35 | 55.61 ± 3.23 | 50.50 ± 1.79 |
| IVCT (ms) | 22.07 ± 2.58 | 18.80 ± 0.77 | 19.66 ± 1.37 | 17.52 ± 0.58 |
| IVRT (ms) | 23.56 ± 1.16 | 23.38 ± 0.62 | 23.44 ± 1.87 | 23.35 ± 0.74 |
| MVA (mm·s$^{-1}$) | 424.75 ± 32.39 | 404.12 ± 36.93 | 327.49 ± 38.21 | 372.43 ± 17.76 |
| MVE (mm·s$^{-1}$) | 651.45 ± 42.23 | 621.88 ± 60.19 | 619.20 ± 40.46 | 603.69 ± 28.06 |
| MVET (ms) | 54.45 ± 3.42 | 58.42 ± 2.03 | 49.04 ± 3.27 | 60.08 ± 2.86 |
| MV E/A | 1.52 ± 0.11 | 1.54 ± 0.10 | 1.88 ± 0.15* | 1.63 ± 0.05 |

*Note*: Results are expressed as mean ± SEM.

Abbreviations: AET, aortic ejection time; Ang II, angiotensin II; ApoE, apolipoprotein-E; bpm, beats per minute; CHOP, C/EBP homologous protein; EF, ejection fraction; FS, fractional shortening; HR, heart rate; IVCT, isovolumetric contraction time; IVRT, isovolumetric relaxation time; IVS, interventricular septum; KO, knockout; LV, left ventricular; LVAW, LV anterior wall thickness; LVID, LV internal diameter; LVPW, LV posterior wall thickness; MVA, mitral valve peak A; MVE, mitral valve peak E; MVET, mitral valve ejection time.

*$P < 0.05$ versus saline and double KO + saline.

#$P < 0.05$ versus ApoE$^{-/-}$/CHOP$^{+/+}$ + Ang II group (one-way ANOVA).

ERN1–XBP1 branch, thus confirming that the crosstalk between mitochondrial dysfunction and ER stress operates in experimental AAA and suggesting that the attenuation of ER stress could contribute, at least in a part, to the favourable response elicited by SS31 on AAA. In fact, our recent studies in a large cohort of AAA patients consistently demonstrated the induction of ER stress in human disease (Navas-Madroñal et al., 2019) and, here, we confirmed this relationship in experimental aneurysm as has been recently corroborated in a proteomic analysis (Morgan et al., 2022).

Previous studies showed that inhibitors of ER stress, such as TUDCA and PBA, ameliorated aneurysm diameter in Ang II-infused ApoE$^{-/-}$ mice (Ni et al., 2018; Qin et al., 2017). These studies basically focused on the effect of ER stress inhibition on aneurysm formation; however, here, we performed an exhaustive analysis of the impact of ER stress inhibition on disease development, severity and survival and on critical processes for AAA development such as inflammation and MMP activation. In the present study, we confirmed the benefit of these drugs on AAA development under our experimental conditions, expanded the research to analyse the resemblance with the response exerted by SS31 and refined our understanding of the consequences of ER stress inhibition on aneurysmal disease. This thorough analysis revealed that TUDCA diminished Ang II-induced mortality to a similar extent than SS31, whereas PBA only delayed death episodes. Both SS31 and ER stress inhibition comparably improved the severity of AAA.

In contrast with SS31 and with previous studies (Ni et al., 2018; Qin et al., 2017), ER stress inhibitors significantly reduced the Ang II-mediated increase in SBP by about 10 mmHg, although mice remained hypertensive. Considering that Ang II-induced AAA in ApoE$^{-/-}$ mice is largely independent of the Ang II vasopressor function (Cassis et al., 2009), it is unlikely that the reduction in blood pressure induced by ER stress inhibition could underlie the benefit of this intervention on aneurysm expansion.

The impact of SS31 and ER stress inhibitors on the striking ECM disorganization induced by Ang II was also comparable. Moreover, the increased vascular expression of MMP2 and MMP9 was markedly attenuated by SS31 and TUDCA, whereas PBA only impacted on MMP9. To our knowledge, this is the first report addressing the

consequences of SS31 or ER stress inhibitors on vascular MMP expression although this peptide abrogates the enhanced MMP9 levels found in a model of cigarette smoke-induced airway inflammation (Yang et al., 2021).

Likewise, vascular inflammatory infiltration induced by Ang II was markedly decreased by SS31 and ER stress inhibition coupled to a significant attenuation of the vascular expression of inflammatory markers. Consistently, it has been reported that SS31 limits systemic inflammation and macrophage content in atherosclerotic plaques from high-fat diet-fed ApoE KO mice (M. Zhang et al., 2017). Because the immune response has emerged as a promising target to limit AAA (Paige et al., 2019; Rateri et al., 2011), overall, the reduction of vascular inflammation provided by SS31 could be critically involved in its beneficial impact on aneurysm development. Likewise, our data show that, virtually, the inhibition of AAA by SS31 mimics that triggered by ER stress inhibitors.

Prolonged ER stress results in a dysregulation of the UPR and apoptosis orchestrated by CHOP. Apoptosis is a key factor that contributes to medial degeneration in AAA (Thompson et al., 1997), as we and others have reported in humans and animal models (Navas-Madroñal et al., 2019; Ni et al., 2018; Qin et al., 2017). Interestingly, the expression of CHOP is strikingly increased in aneurysmal samples and attenuated by both SS31 and TUDCA, in agreement with previous in vitro data in leukocytes from diabetic patients in which this peptide restored *CHOP* mRNA levels (Escribano-López et al., 2019). We found that CHOP deletion in Ang II-infused ApoE$^{-/-}$ mice limited abdominal aortic dilation associated with a reduction in AAA incidence and severity, as previously reported for CHOP KO mice subjected to thoracic aortic aneurysm (Jia et al., 2017). However, *Chop* knockdown neither improved survival nor vascular inflammation. These data and that obtained with ER stress inhibitors suggest that, although CHOP plays a relevant role in AAA, all the UPR branches contribute to this disorder. Deletion of *Chop* did not affect the Ang II-mediated induction of ER stress markers, probably because *Chop* is a downstream signalling effector of the three signalling branches of the UPR. Finally, *Chop* knockdown led to a reduction in the Ang II-mediated increase of blood pressure, in line with the response induced by ER stress inhibitors, suggesting that a common mechanism could underlie this behaviour.

Ang II is also closely associated with the pathogenesis of cardiac hypertrophy (Frieler & Mortensen, 2015; Kawano et al., 2005; Kurdi & Booz, 2011). In fact, in ApoE$^{-/-}$ mice, Ang II disturbs cardiac function and induces cardiac hypertrophy. We found that these abnormalities were accompanied by an induction of hypertrophic and ER stress markers, as previously reported (Hamid et al., 2011; Li et al., 2019; J. S. Zhang et al., 2016). Additionally, not only the activation of ER stress but also the impairment of mitochondrial function is known to contribute to these maladaptive responses (Mervaala et al., 2010; Prola et al., 2019; Wang et al., 2017). In this context, we have observed that, in Ang II-infused ApoE$^{-/-}$ mice, TUDCA partially protected from these deleterious effects by reducing cardiac hypertrophy in agreement with previous reports (Li et al., 2018; Rani et al., 2017), whereas a comparable benefit was achieved by SS31. Both SS31 and TUDCA significantly ameliorated the up-regulation of some hypertrophic markers, supporting once more their cardioprotective effects. Likewise, our data demonstrate that the treatment with TUDCA, SS31 and even with SS20 improved diastolic function. A protective effect of SS31 against cardiac ischaemia–reperfusion injury and **doxorubicin**-induced cardiotoxicity has been recently reported (W. Zhang et al., 2019; L. Zhang, Feng, et al., 2021) and the benefit of SS20 on heart function in response to Ang II is supported by the literature (Dai et al., 2013). Our data reinforce the cardioprotective role of SS31 and sustain its benefit against the deleterious responses exerted by Ang II. Of interest, the lack of CHOP greatly protected from myocardial hypertrophic remodelling in response to Ang II and normalized systolic function. Because TUDCA and SS31 prevented the cardiac up-regulation of CHOP induced by Ang II in hypertrophic hearts, this effect could account for the favourable response triggered by both compounds.

It should be highlighted that SS31 and TUDCA exhibit a more favourable outcome than PBA at both the vascular and cardiac levels. Certainly, besides the significant increase in survival in the aneurysmal aorta, SS31 and TUDCA exerted a more efficacious effect by limiting MMP activity, inflammation and cardiac remodelling than that triggered by PBA. The antioxidant properties of SS31 and the low impact of ER stress inhibitors on mitochondrial dysfunction could explain these differences. Clinical trials have demonstrated the therapeutic effects and safety of SS31 and TUDCA in humans (Kusaczuk, 2019; Szeto, 2019). SS31 has been shown to be effective for acute kidney injury and ischaemia–reperfusion-derived organ damage (Dai et al., 2013), whereas TUDCA is indicated for the treatment of liver cirrhosis, primary biliary cholangitis and insulin resistance (Kusaczuk, 2019). Therefore, SS31 and TUDCA emerge as valuable therapeutic tools for the management of AAA.

We are aware of the limitations of our present study. As commented above, the specific weight that each of the responses triggered by SS31 (the inhibition of ER stress but also the blockade of both mitochondrial dysfunction and oxidative stress) has in preventing experimental AAA cannot be determined. However, considering our previous data on human AAA (Navas-Madroñal et al., 2019), we point out that the maintenance of mitochondrial homeostasis and the blockade of ER stress would be part of the main mechanisms underlying the favourable impact of SS31 on aneurysm development.

In summary, we have shown that SS31, a specific inhibitor of mitochondrial stress, limits aneurysm progression and exhibits cardioprotective effects. Our data suggest that the antioxidant properties of SS31 coupled with its anti-inflammatory effects and the inhibition of ER stress could account for the improvement in ECM destructive remodelling and inflammation underlying the therapeutic benefit of this drug. Therapeutic strategies to reduce mitochondrial stress and alleviate ER stress may hold the promise to reduce the high morbidity and mortality associated with AAA and cardiac hypertrophy.

## AUTHOR CONTRIBUTIONS

**Miquel Navas-Madroñal:** Data curation (lead); formal analysis (lead); investigation (equal); methodology (equal); project administration

(supporting); software (lead); validation (supporting); visualization (equal); writing—original draft (equal); writing—review and editing (supporting). **Rafael Antonio Almendra-Pegueros:** Data curation (equal); formal analysis (supporting); methodology (equal); software (equal); writing—review and editing (equal). **Lidia Puertas-Umbert:** Data curation (equal); methodology (equal); software (supporting); writing—original draft (supporting). **Francesc Jimenez-Altayo:** Conceptualization (supporting); data curation (equal); formal analysis (supporting); methodology (supporting); software (supporting); supervision (supporting); writing—original draft (supporting); writing—review and editing (supporting). **Josep Julve:** Data curation (equal); formal analysis (equal); investigation (supporting); methodology (equal); resources (equal); writing—original draft (supporting); writing—review and editing (equal). **Belen Perez:** Data curation (equal); formal analysis (equal); methodology (supporting); writing—original draft (supporting); writing—review and editing (supporting). **Marta Consegal-Pérez:** Data curation (equal); formal analysis (equal); methodology (supporting); writing—original draft (supporting). **Modar Kassan:** Conceptualization (supporting); investigation (supporting); methodology (supporting); validation (equal); visualization (equal); writing—original draft (supporting). **Jose Martínez-González:** Conceptualization (supporting); methodology (supporting); validation (supporting); visualization (supporting); writing—original draft (supporting); writing—review and editing (supporting). **Cristina Rodríguez:** Conceptualization (equal); formal analysis (supporting); funding acquisition (equal); investigation (equal); methodology (equal); project administration (lead); resources (supporting); validation (equal); visualization (equal); writing—original draft (lead); writing—review and editing (lead). **María Galán:** Conceptualization (lead); data curation (lead); formal analysis (lead); funding acquisition (lead); investigation (lead); methodology (lead); project administration (lead); resources (lead); software (equal); supervision (lead); validation (lead); visualization (lead); writing—original draft (lead); writing—review and editing (lead).

## ACKNOWLEDGEMENTS

This work was funded by grants from the Instituto de Salud Carlos III (ISCIII) (grants PI17/01837 and PI20/01004 to M.G. and PI21/01048 to C.R.). M.N.-M. was supported by a contract associated to a Miguel Servet project (CP15/00126). R.A.-P. and L.P.-U. are supported by a PFIS fellowship (FI21/00125 and FI19/00331, respectively; ISCIII). M. G. was hired under the Miguel Servet Programme (ISCIII; Refs CP15/00126 and CP20/01004).

## CONFLICT OF INTEREST STATEMENT

The authors have declared that no conflict of interest exists.

## DECLARATION OF TRANSPARENCY AND SCIENTIFIC RIGOUR

This Declaration acknowledges that this paper adheres to the principles for transparent reporting and scientific rigour of preclinical research as stated in the *BJP* guidelines for Natural Products Research, Design and Analysis, Immunoblotting and Immunochemistry, and Animal Experimentation, and as recommended by funding agencies, publishers and other organizations engaged with supporting research.

## DATA AVAILABILITY STATEMENT

The data that support the findings of this study are available from the corresponding authors upon reasonable request. Some data may not be made available because of privacy or ethical restrictions.

## ORCID

*María Galán* https://orcid.org/0000-0002-4758-8388

## REFERENCES

Alexander, S. P., Fabbro, D., Kelly, E., Mathie, A., Peters, J. A., Veale, E. L., Armstrong, J. F., Faccenda, E., Harding, S. D., Pawson, A. J., Southan, C., Davies, J. A., Boison, D., Burns, K. E., Dessauer, C., Gertsch, J., Helsby, N. A., Izzo, A. A., Koesling, D., … Wong, S. S. (2021). The Concise Guide to PHARMACOLOGY 2021/22: Enzymes. *British Journal of Pharmacology*, *178*(S1), S313–S411. https://doi.org/10.1111/bph.15542

Alexander, S. P., Kelly, E., Mathie, A., Peters, J. A., Veale, E. L., Armstrong, J. F., Faccenda, E., Harding, S. D., Pawson, A. J., Southan, C., Buneman, O. P., Cidlowski, J. A., Christopoulos, A., Davenport, A. P., Fabbro, D., Spedding, M., Striessnig, J., Davies, J. A., Ahlers-Dannen, K. E., … Zolghadri, Y. (2021). The Concise Guide to PHARMACOLOGY 2021/22: Other protein targets. *British Journal of Pharmacology*, *178*(S1), S1–S26. https://doi.org/10.1111/bph.15537

Alexander, S. P. H., Roberts, R. E., Broughton, B. R. S., Sobey, C. G., George, C. H., Stanford, S. C., Cirino, G., Docherty, J. R., Giembycz, M. A., Hoyer, D., Insel, P. A., Izzo, A. A., Ji, Y., MacEwan, D. J., Mangum, J., Wonnacott, S., & Ahluwalia, A. (2018). Goals and practicalities of immunoblotting and immunohistochemistry: A guide for submission to the *British Journal of Pharmacology*. *British Journal of Pharmacology*, *175*(3), 407–411. https://doi.org/10.1111/bph.14112

Bath, M. F., Gokani, V. J., Sidloff, D. A., Jones, L. R., Choke, E., Sayers, R. D., & Bown, M. J. (2015). Systematic review of cardiovascular disease and cardiovascular death in patients with a small abdominal aortic aneurysm. *The British Journal of Surgery*, *102*(8), 866–872. https://doi.org/10.1002/bjs.9837

Baxter, B. T., Matsumura, J., Curci, J. A., McBride, R., Larson, L., Blackwelder, W., Lam, D., Wijesinha, M., Terrin, M., & for the N-TA3CT Investigators. (2020). Effect of doxycycline on aneurysm growth among patients with small infrarenal abdominal aortic aneurysms: A randomized clinical trial. *Journal of the American Medical Association*, *323*(20), 2029–2038. https://doi.org/10.1001/jama.2020.5230

Cai, J., Jiang, Y., Zhang, M., Zhao, H., Li, H., Li, K., Zhang, X., & Qiao, T. (2018). Protective effects of mitochondrion-targeted peptide SS-31 against hind limb ischemia-reperfusion injury. *Journal of Physiology and Biochemistry*, *74*(2), 335–343. https://doi.org/10.1007/s13105-018-0617-1

Cassis, L. A., Gupte, M., Thayer, S., Zhang, X., Charnigo, R., Howatt, D. A., Rateri, D. L., & Daugherty, A. (2009). ANG II infusion promotes abdominal aortic aneurysms independent of increased blood pressure in hypercholesterolemic mice. *American Journal of Physiology. Heart and Circulatory Physiology*, *296*, H1660–H1665. https://doi.org/10.1152/ajpheart.00028.2009

Curtis, M. J., Alexander, S. P. H., Cirino, G., George, C. H., Kendall, D. A., Insel, P. A., Izzo, A. A., Ji, Y., Panettieri, R. A., Patel, H. H., Sobey, C. G., Stanford, S. C., Stanley, P., Stefanska, B., Stephens, G. J., Teixeira, M. M., Vergnolle, N., & Ahluwalia, A. (2022). Planning experiments: Updated guidance on experimental design and analysis and their reporting III. *Br J Pharmacol.*, *179*, 3907–3913. https://doi.org/10.1111/bph.15868

Dai, D. F., Chen, T., Szeto, H., Nieves-Cintrón, M., Kutyavin, V., Santana, L. F., & Rabinovitch, P. S. (2011). Mitochondrial targeted antioxidant peptide ameliorates hypertensive cardiomyopathy. *Journal of the American College of Cardiology*, *58*(1), 73–82. https://doi.org/10.1016/j.jacc.2010.12.044

Dai, D. F., Hsieh, E. J., Chen, T., Menendez, L. G., Basisty, N. B., Tsai, L., Beyer, R. P., Crispin, D. A., Shulman, N. J., Szeto, H. H., Tian, R., MacCoss, M. J., & Rabinovitch, P. S. (2013). Global proteomics and pathway analysis of pressure-overload-induced heart failure and its attenuation by mitochondrial-targeted peptides. *Circulation. Heart Failure*, *6*(5), 1067–1076. https://doi.org/10.1161/CIRCHEARTFAILURE.113.000406

Daugherty, A., Manning, M. W., & Cassis, L. A. (2000). Angiotensin II promotes atherosclerotic lesions and aneurysms in apolipoprotein E-deficient mice. *The Journal of Clinical Investigation*, *105*(11), 1605–1612. https://doi.org/10.1172/JCI7818

Dikalova, A. E., Bikineyeva, A. T., Budzyn, K., Nazarewicz, R. R., McCann, L., Lewis, W., Harrison, D. G., & Dikalov, S. I. (2010). Therapeutic targeting of mitochondrial superoxide in hypertension. *Circulation Research*, *107*, 106–116. https://doi.org/10.1161/CIRCRESAHA.109.214601

Emeto, T. I., Moxon, J. V., Au, M., & Golledge, J. (2016). Oxidative stress and abdominal aortic aneurysm: Potential treatment targets. *Clinical Science (London, England)*, *130*(5), 301–315. https://doi.org/10.1042/CS20150547

Emeto, T. I., Seto, S. W., & Golledge, J. (2014). Targets for medical therapy to limit abdominal aortic aneurysm progression. *Current Drug Targets*, *15*, 860–873. https://doi.org/10.2174/1389450115666140804155036

Escribano-López, I., de Marañon, A. M., Iannantuoni, F., López-Domènech, S., Abad-Jiménez, Z., Díaz, P., Solá, E., Apostolova, N., Rocha, M., & Víctor, V. M. (2019). The mitochondrial antioxidant SS-31 modulates oxidative stress, endoplasmic reticulum stress, and autophagy in type 2 diabetes. *Journal of Clinical Medicine*, *8*(9), 1322. https://doi.org/10.3390/jcm8091322

Forsdahl, S. H., Solberg, S., Singh, K., & Jacobsen, B. K. (2010). Abdominal aortic aneurysms, or a relatively large diameter of non-aneurysmal aortas, increase total and cardiovascular mortality: The Tromsø study. *International Journal of Epidemiology*, *39*(1), 225–232. https://doi.org/10.1093/ije/dyp3

Freiberg, M. S., Arnold, A. M., Newman, A. B., Edwards, M. S., Kraemer, K. L., & Kuller, L. H. (2008). Abdominal aortic aneurysms, increasing infrarenal aortic diameter, and risk of total mortality and incident cardiovascular disease events: 10-year follow-up data from the Cardiovascular Health Study. *Circulation*, *117*(8), 1010–1017. https://doi.org/10.1161/CIRCULATIONAHA.107.720219

Frieler, R. A., & Mortensen, R. M. (2015). Immune cell and other non-cardiomyocyte regulation of cardiac hypertrophy and remodeling. *Circulation*, *131*, 1019–1030. https://doi.org/10.1161/CIRCULATIONAHA.114.008788

Galán, M., Varona, S., Guadall, A., Orriols, M., Navas, M., Aguiló, S., de Diego, A., Navarro, M. A., García-Dorado, D., Rodríguez-Sinovas, A., Martínez-González, J., & Rodriguez, C. (2017). Lysyl oxidase overexpression accelerates cardiac remodeling and aggravates angiotensin II-induced hypertrophy. *The FASEB Journal*, *31*(9), 3787–3799. https://doi.org/10.1096/fj.201601157RR

Galán, M., Varona, S., Orriols, M., Rodríguez, J. A., Aguiló, S., Dilmé, J., Camacho, M., Martínez-González, J., & Rodriguez, C. (2016). Induction of histone deacetylases (HDACs) in human abdominal aortic aneurysm: Therapeutic potential of HDAC inhibitors. *Disease Models & Mechanisms*, *9*(5), 541–552. https://doi.org/10.1242/dmm.024513

GBD. (2015). Mortality and Causes of Death Collaborators. Global, regional, and national age-sex specific all-cause and cause-specific mortality for 240 causes of death, 1990–2013: A systematic analysis for the Global Burden of Disease Study 2013. *Lancet*, *385*, 117–171. https://doi.org/10.1016/S0140-6736(14)61682-2

Giorgi, C., De Stefani, D., Bononi, A., Rizzuto, R., & Pinton, P. (2009). Structural and functional link between the mitochondrial network and the endoplasmic reticulum. *The International Journal of Biochemistry & Cell Biology*, *41*, 1817–1827. https://doi.org/10.1016/j.biocel.2009.04.010

Golledge, J. (2019). Abdominal aortic aneurysm: Update on pathogenesis and medical treatments. *Nature Reviews. Cardiology*, *16*, 225–242. https://doi.org/10.1038/s41569-018-0114-9

Guzik, B., Sagan, A., Ludew, D., Mrowiecki, W., Chwała, M., Bujak-Gizycka, B., Filip, G., Grudzien, G., Kapelak, B., Zmudka, K., Mrowiecki, T., Sadowski, J., Korbut, R., & Guzik, T. J. (2013). Mechanisms of oxidative stress in human aortic aneurysms-association with clinical risk factors for atherosclerosis and disease severity. *International Journal of Cardiology*, *168*(3), 2389–2396. https://doi.org/10.1016/j.ijcard.2013.01.278

Hamid, T., Guo, S. Z., Kingery, J. R., Xiang, X., Dawn, B., & Prabhu, S. D. (2011). Cardiomyocyte NF-κB p65 promotes adverse remodelling, apoptosis, and endoplasmic reticulum stress in heart failure. *Cardiovascular Research*, *89*(1), 129–138. https://doi.org/10.1093/cvr/cvq274

Hetz, C., Zhang, K., & Kaufman, R. J. (2020). Mechanisms, regulation and functions of the unfolded protein response. *Nature Reviews. Molecular Cell Biology*, *21*(8), 421–438. https://doi.org/10.1038/s41580-020-0250-z

Jia, L. X., Zhang, W. M., Li, T. T., Liu, Y., Piao, C. M., Ma, Y. C., Lu, Y., Wang, Y., Liu, T. T., Qi, Y. F., & Du, J. (2017). ER stress dependent microparticles derived from smooth muscle cells promote endothelial dysfunction during thoracic aortic aneurysm and dissection. *Clinical Science (London, England)*, *131*(12), 1287–1299. https://doi.org/10.1042/CS20170252

Kassan, M., Galan, M., Partyka, M., Saifudeen, Z., Henrion, D., Trebak, M., & Matrougui, K. (2012). Endoplasmic reticulum stress is involved in cardiac damage and vascular endothelial dysfunction in hypertensive mice. *Arteriosclerosis, Thrombosis, and Vascular Biology*, *32*, 1652–1661. https://doi.org/10.1161/ATVBAHA.112.249318

Kawano, S., Kubota, T., Monden, Y., Kawamura, N., Tsutsui, H., Takeshita, A., & Sunagawa, K. (2005). Blockade of NF-κB ameliorates myocardial hypertrophy in response to chronic infusion of angiotensin II. *Cardiovascular Research*, *67*, 689–698. https://doi.org/10.1016/j.cardiores.2005.04.030

Kleele, T., Rey, T., Winter, J., Zaganelli, S., Mahecic, D., Perreten Lambert, H., Ruberto, F. P., Nemir, M., Wai, T., Pedrazzini, T., & Manley, S. (2021). Distinct fission signatures predict mitochondrial degradation or biogenesis. *Nature*, *593*(7859), 435–439. https://doi.org/10.1038/s41586-021-03510-6

Klink, A., Hyafil, F., Rudd, J., Faries, P., Fuster, V., Mallat, Z., Meilhac, O., Mulder, W. J., Michel, J. B., Ramirez, F., Storm, G., Thompson, R., Turnbull, I. C., Egido, J., Martín-Ventura, J. L., Zaragoza, C., Letourneur, D., & Fayad, Z. A. (2011). Diagnostic and therapeutic strategies for small abdominal aortic aneurysms. *Nature Reviews. Cardiology*, *8*(6), 338–347. https://doi.org/10.1038/nrcardio.2011.1

Kloner, R. A., Shi, J., & Dai, W. (2015). New therapies for reducing post-myocardial left ventricular remodeling. *Annals of Translational Medicine*, *3*(2), 20. https://doi.org/10.3978/j.issn.2305-5839.2015.01.13

Kuivaniemi, H., Ryer, E. J., Elmore, J. R., & Tromp, G. (2015). Understanding the pathogenesis of abdominal aortic aneurysms. *Expert Review of Cardiovascular Therapy*, *13*, 975–987. https://doi.org/10.1586/14779072.2015.1074861

Kurdi, M., & Booz, G. W. (2011). New take on the role of angiotensin II in cardiac hypertrophy and fibrosis. *Hypertension*, *57*, 1034–1038. https://doi.org/10.1161/HYPERTENSIONAHA.111.172700

Kusaczuk, M. (2019). Tauroursodeoxycholate-bile acid with chaperoning activity: Molecular and cellular effects and therapeutic perspectives. *Cell*, *8*(12), 1471. https://doi.org/10.3390/cells8121471

Laurindo, F. R., Fernandes, D. C., & Santos, C. X. (2008). Assessment of superoxide production and NADPH oxidase activity by HPLC analysis of dihydroethidium oxidation products. *Methods in Enzymology*, *441*, 237–260. https://doi.org/10.1016/S0076-6879(08)01213-5

Li, J., Kemp, B. A., Howell, N. L., Massey, J., Mińczuk, K., Huang, Q., Chordia, M. D., Roy, R. J., Patrie, J. T., Davogustto, G. E., Kramer, C. M., Epstein, F. H., Carey, R. M., Taegtmeyer, H., Keller, S. R., & Kundu, B. K. (2019). Metabolic changes in spontaneously hypertensive rat hearts precede cardiac dysfunction and left ventricular hypertrophy. *Journal of the American Heart Association*, *8*(4), e010926. https://doi.org/10.1161/JAHA.118.010926

Li, J., Yue, G., Ma, W., Zhang, A., Zou, J., Cai, Y., Tang, X., Wang, J., Liu, J., Li, H., & Su, H. (2018). Ufm1-specific ligase Ufl1 regulates endoplasmic reticulum homeostasis and protects against heart failure. *Circulation. Heart Failure*, *11*(10), e004917. https://doi.org/10.1161/CIRCHEARTFAILURE.118.004917

Lilley, E., Stanford, S. C., Kendall, D. E., Alexander, S. P., Cirino, G., Docherty, J. R., George, C. H., Insel, P. A., Izzo, A. A., Ji, Y., Panettieri, R. A., Sobey, C. G., Stefanska, B., Stephens, G., Teixeira, M., & Ahluwalia, A. (2020). ARRIVE 2.0 and the *British Journal of Pharmacology*: Updated guidance for 2020. *British Journal of Pharmacology*, *177*(16), 3611–3616. https://doi.org/10.1111/bph.15178

Lu, H. I., Huang, T. H., Sung, P. H., Chen, Y. L., Chua, S., Chai, H. Y., Chung, S. Y., Liu, C. F., Sun, C. K., Chang, H. W., Zhen, Y. Y., Lee, F. Y., & Yip, H. K. (2016). Administration of antioxidant peptide SS-31 attenuates transverse aortic constriction-induced pulmonary arterial hypertension in mice. *Acta Pharmacologica Sinica*, *37*(5), 589–603. https://doi.org/10.1038/aps.2015.162

Malhotra, J. D., & Kaufman, R. J. (2007). Endoplasmic reticulum stress and oxidative stress: A vicious cycle or a double-edged sword? *Antioxidants & Redox Signaling*, *9*, 2277–2293. https://doi.org/10.1089/ars.2007.1782

Manning, M. W., Cassi, L. A., Huang, J., Szilvassy, S. J., & Daugherty, A. (2002). Abdominal aortic aneurysms: Fresh insights from a novel animal model of the disease. *Vascular Medicine*, *7*(1), 45–54. https://doi.org/10.1191/1358863x02vm413ra

Mervaala, E., Biala, A., Merasto, S., Lempiäinen, J., Mattila, I., Martonen, E., Eriksson, O., Louhelainen, M., Finckenberg, P., Kaheinen, P., Muller, D. N., Luft, F. C., Lapatto, R., & Oresic, M. (2010). Metabolomics in angiotensin II-induced cardiac hypertrophy. *Hypertension*, *55*(2), 508–515. https://doi.org/10.1161/HYPERTENSIONAHA.109.145490

Morgan, S., Lee, L. H., Halu, A., Nicolau, J. S., Higashi, H., Ha, A. H., Wen, J. R., Daugherty, A., Libby, P., Cameron, S. J., Mix, D., Aikawa, E., Owens, A. P. 3rd., Singh, S. A., & Aikawa, M. (2022). Identifying novel mechanisms of abdominal aortic aneurysm via unbiased proteomics and systems biology. *Frontiers in Cardiovascular Medicine*, *9*, 889994. https://doi.org/10.3389/fcvm.2022.889994

Navas-Madroñal, M., Rodriguez, C., Kassan, M., Fité, J., Escudero, J. R., Cañes, L., Martínez-González, J., Camacho, M., & Galán, M. (2019). Enhanced endoplasmic reticulum and mitochondrial stress in abdominal aortic aneurysm. *Clinical Science (London, England)*, *133*(13), 1421–1438. https://doi.org/10.1042/CS20190399

Ni, X. Q., Lu, W. W., Zhang, J. S., Zhu, Q., Ren, J. L., Yu, Y. R., Liu, X. Y., Wang, X. J., Han, M., Jing, Q., Du, J., Tang, C. S., & Qi, Y. F. (2018). Inhibition of endoplasmic reticulum stress by intermedin1-53 attenuates angiotensin II-induced abdominal aortic aneurysm in ApoE KO mice. *Endocrine*, *62*(1), 90–106. https://doi.org/10.1007/s12020-018-1657-6

Nickel, A. G., von Hardenberg, A., Hohl, M., Löffler, J. R., Kohlhaas, M., Becker, J., Reil, J. C., Kazakov, A., Bonnekoh, J., Stadelmaier, M., Puhl, S. L., Wagner, M., Bogeski, I., Cortassa, S., Kappl, R., Pasieka, B., Lafontaine, M., Lancaster, C. R., Blacker, T. S., … Maack, C. (2015). Reversal of mitochondrial transhydrogenase causes oxidative stress in heart failure. *Cell Metabolism*, *22*(3), 472–484. https://doi.org/10.1016/j.cmet.2015.07.0

Nordon, I. M., Hinchliffe, R. J., Loftus, I. M., & Thompson, M. M. (2011). Pathophysiology and epidemiology of abdominal aortic aneurysms. *Nature Reviews. Cardiology*, *8*, 92–102. https://doi.org/10.1038/nrcardio.2010.180

Paige, E., Clément, M., Lareyre, F., Sweeting, M., Raffort, J., Grenier, C., Finigan, A., Harrison, J., Peters, J. E., Sun, B. B., Butterworth, A. S., Harrison, S. C., Bown, M. J., Lindholt, J. S., Badger, S. A., Kullo, I. J., Powell, J., Norman, P. E., Scott, D. J. A., … Mallat, Z. (2019). Interleukin-6 receptor signaling and abdominal aortic aneurysm growth rates. *Circulation: Genomic and Precision Medicine*, *12*(2), e002413. https://doi.org/10.1161/CIRCGEN.118.002413

Percie du Sert, N., Hurst, V., Ahluwalia, A., Alam, S., Avey, M. T., Baker, M., Browne, W. J., Clark, A., Cuthill, I. C., Dirnagl, U., Emerson, M., Garner, P., Holgate, S. T., Howells, D. W., Karp, N. A., Lazic, S. E., Lidster, K., MacCallum, C. J., Macleod, M., … Würbel, H. (2020). The ARRIVE guidelines 2.0: Updated guidelines for reporting animal research. *PLoS Biology*, *18*(7), e3000410. https://doi.org/10.1371/journal.pbio.3000410

Potteaux, S., & Tedgui, A. (2015). Monocytes, macrophages and other inflammatory mediators of abdominal aortic aneurysm. *Current Pharmaceutical Design*, *21*, 4007–4015. https://doi.org/10.2174/1381612821666150826093855

Prola, A., Nichtova, Z., Pires da Silva, J., Piquereau, J., Monceaux, K., Guilbert, A., Gressette, M., Ventura-Clapier, R., Garnier, A., Zahradnik, I., Novotova, M., & Lemaire, C. (2019). Endoplasmic reticulum stress induces cardiac dysfunction through architectural modifications and alteration of mitochondrial function in cardiomyocytes. *Cardiovascular Research*, *115*(2), 328–342. https://doi.org/10.1093/cvr/cvy197

Qin, Y., Wang, Y., Liu, O., Jia, L., Fang, W., Du, J., & Wei, Y. (2017). Tauroursodeoxycholic acid attenuates angiotensin II induced abdominal aortic aneurysm formation in apolipoprotein E-deficient mice by inhibiting endoplasmic reticulum stress. *European Journal of Vascular and Endovascular Surgery*, *53*(3), 337–345. https://doi.org/10.1016/j.ejvs.2016.10.026

Rani, S., Sreenivasaiah, P. K., Kim, J. O., Lee, M. Y., Kang, W. S., Kim, Y. S., Ahn, Y., Park, W. J., Cho, C., & Kim, D. H. (2017). Tauroursodeoxycholic acid (TUDCA) attenuates pressure overload-induced cardiac remodeling by reducing endoplasmic reticulum stress. *PLoS ONE*, *12*(4), e0176071. https://doi.org/10.1371/journal.pone.0176071

Rateri, D. L., Howatt, D. A., Moorleghen, J. J., Charnigo, R., Cassis, L. A., & Daugherty, A. (2011). Prolonged infusion of angiotensin II in *apoE*$^{-/-}$ mice promotes macrophage recruitment with continued expansion of abdominal aortic aneurysm. *The American Journal of Pathology*, *179*(3), 1542–1548. https://doi.org/10.1016/j.ajpath.2011.05.049

Samson, R. (2012). Can pharmacologic agents slow abdominal aortic aneurysm growth? *Seminars in Vascular Surgery*, *25*, 25–28. https://doi.org/10.1053/j.semvascsurg.2012.03.004

Sánchez-Infantes, D., Nus, M., Navas-Madroñal, M., Fité, J., Pérez, B., Barros-Membrilla, A. J., Soto, B., Martínez-González, J., Camacho, M., Rodriguez, C., Mallat, Z., & Galán, M. (2021). Oxidative stress and inflammatory markers in abdominal aortic aneurysm. *Antioxidants (Basel).*, *10*(4), 602. https://doi.org/10.3390/antiox10040602

Shimizu, K., Mitchell, R. N., & Libby, P. (2006). Inflammation and cellular immune responses in abdominal aortic aneurysms. *Arteriosclerosis, Thrombosis, and Vascular Biology*, *26*, 987–994. https://doi.org/10.1161/01.ATV.0000214999.12921.4f

Szeto, H. H. (2008). Mitochondria-targeted cytoprotective peptides for ischemia-reperfusion injury. *Antioxidants & Redox Signaling*, *10*(3), 601–619. https://doi.org/10.1089/ars.2007.1892

Szeto, H. H. (2019). Stealth peptides target cellular powerhouses to fight rare and common age-related diseases. *Protein and Peptide Letters*, *25*(12), 1108–1123. https://doi.org/10.2174/0929866525666181101105209

Tabas, I., & Ron, D. (2011). Integrating the mechanisms of apoptosis induced by endoplasmic reticulum stress. *Nature Cell Biology*, *13*, 184–190. https://doi.org/10.1038/ncb0311-184

Thompson, R. W., Liao, S., & Curci, J. A. (1997). Vascular smooth muscle cell apoptosis in abdominal aortic aneurysms. *Coronary Artery Disease*, *8*, 623–632. https://doi.org/10.1097/00019501-199710000-00005

Timmins, J. M., Ozcan, L., Seimon, T. A., Li, G., Malagelada, C., Backs, J., Backs, T., Bassel-Duby, R., Olson, E. N., Anderson, M. E., & Tabas, I. (2009). Calcium/calmodulin-dependent protein kinase II links ER stress with Fas and mitochondrial apoptosis pathways. *The Journal of Clinical Investigation*, *119*, 2925–2941. https://doi.org/10.1172/JCI38857

Torres-Fonseca, M., Galan, M., Martinez-Lopez, D., Cañes, L., Roldan-Montero, R., Alonso, J., Reyero-Postigo, T., Orriols, M., Mendez-Barbero, N., Sirvent, M., Blanco-Colio, L. M., Martínez, J., Martin-Ventura, J. L., Rodríguez, C., & En representación del Grupo de trabajo de Biología Vascular de la Sociedad Española de Arteriosclerosis. (2019). Pathophisiology of abdominal aortic aneurysm: Biomarkers and novel therapeutic targets. *Clínica e Investigación en Arteriosclerosis (English Edition)*, *31*(4), 166–177. https://doi.org/10.1016/j.arteri.2018.10.002

Ulug, P., Powell, J. T., Martinez, M. A., Ballard, D. J., & Filardo, G. (2020). Surgery for small asymptomatic abdominal aortic aneurysms. *Cochrane Database of Systematic Reviews*, *7*(7), CD001835. https://doi.org/10.1002/14651858.CD001835.pub5

Usui, F., Shirasuna, K., Kimura, H., Tatsumi, K., Kawashima, A., Karasawa, T., Yoshimura, K., Aoki, H., Tsutsui, H., Noda, T., Sagara, J., Taniguchi, S., & Takahashi, M. (2015). Inflammasome activation by mitochondrial oxidative stress in macrophages leads to the development of angiotensin II-induced aortic aneurysm. *Arteriosclerosis, Thrombosis, and Vascular Biology*, *35*(1), 127–136. https://doi.org/10.1161/ATVBAHA.114.303763

Wang, Y., Wang, Y. L., Huang, X., Yang, Y., Zhao, Y. J., Wei, C. X., & Zhao, M. (2017). Ibutilide protects against cardiomyocytes injury via inhibiting endoplasmic reticulum and mitochondrial stress pathways. *Heart and Vessels*, *32*(2), 208–215. https://doi.org/10.1007/s00380-016-0891-1

Weintraub, N. L. (2009). Understanding abdominal aortic aneurysm. *The New England Journal of Medicine*, *361*, 1114–1116. https://doi.org/10.1056/NEJMcibr0905244

Yang, D. Q., Zuo, Q. N., Wang, T., Xu, D., Lian, L., Gao, L. J., Wan, C., Chen, L., Wen, F. Q., & Shen, Y. C. (2021). Mitochondrial-targeting antioxidant SS-31 suppresses airway inflammation and oxidative stress induced by cigarette smoke. *Oxidative Medicine and Cellular Longevity*, *2021*, 6644238. https://doi.org/10.1155/2021/6644238

Zhang, J., Wang, P., Wu, Y., Zhu, Y., Peng, X. Y., Xiang, X. M., Xue, M. Y., Li, Q. H., Li, J. X., Yan, Q. G., Liu, L. M., & Li, T. (2021). Role of AQP3 in the vascular leakage of sepsis and the protective effect of Ss-31. *Journal of Cardiovascular Pharmacology*, *78*(2), 280–287. https://doi.org/10.1097/FJC.0000000000001050

Zhang, J. S., Hou, Y. L., Lu, W. W., Ni, X. Q., Lin, F., Yu, Y. R., Tang, C. S., & Qi, Y. F. (2016). Intermedin (1-53) protects against myocardial fibrosis by inhibiting endoplasmic reticulum stress and inflammation induced by homocysteine in apolipoprotein E-deficient mice. *Journal of Atherosclerosis and Thrombosis*, *23*(11), 1294–1306. https://doi.org/10.5551/jat.34082

Zhang, L., Feng, M., Wang, X., Zhang, H., Ding, J., Cheng, Z., & Qian, L. (2021). Peptide Szeto-Schiller 31 ameliorates doxorubicin-induced cardiotoxicity by inhibiting the activation of the p38 MAPK signaling pathway. *International Journal of Molecular Medicine*, *47*(4), 63. https://doi.org/10.3892/ijmm.2021.4896

Zhang, M., Zhao, H., Cai, J., Li, H., Wu, Q., Qiao, T., & Li, K. (2017). Chronic administration of mitochondrion-targeted peptide SS-31 prevents atherosclerotic development in ApoE knockout mice fed Western diet. *PLoS ONE*, *12*(9), e0185688. https://doi.org/10.1371/journal.pone.0185688

Zhang, W., Tam, J., Shinozaki, K., Yin, T., Lampe, J. W., Becker, L. B., & Kim, J. (2019). Increased survival time with SS-31 after prolonged cardiac arrest in rats. *Heart, Lung & Circulation*, *28*(3), 505–508. https://doi.org/10.1016/j.hlc.2018.01.008

Zhao, K., Zhao, G. M., Wu, D., Soong, Y., Birk, A. V., Schiller, P. W., & Szeto, H. H. (2004). Cell-permeable peptide antioxidants targeted to inner mitochondrial membrane inhibit mitochondrial swelling, oxidative cell death, and reperfusion injury. *The Journal of Biological Chemistry*, *279*(33), 34682–34690. https://doi.org/10.1074/jbc.M402999200

## SUPPORTING INFORMATION

Additional supporting information can be found online in the Supporting Information section at the end of this article.

**How to cite this article:** Navas-Madroñal, M., Almendra-Pegueros, R., Puertas-Umbert, L., Jiménez-Altayó, F., Julve, J., Pérez, B., Consegal-Pérez, M., Kassan, M., Martínez-González, J., Rodriguez, C., & Galán, M. (2023). Targeting mitochondrial stress with Szeto-Schiller 31 prevents experimental abdominal aortic aneurysm: Crosstalk with endoplasmic reticulum stress. *British Journal of Pharmacology*, *180*(17), 2230–2249. https://doi.org/10.1111/bph.16077